BRNO UNIVERSITY OF TECHNOLOGY

FACULTY OF ELECTRICAL ENGINEERING AND COMMUNICATION

DEPARTMENT OF POWER ELECTRICAL AND ELECTRONIC ENGINEERING

OPTIMAL FILL FACTOR OF SLOT WITH RESPECT OF USED INSULATION OF MOTOR AND DUTY

MASTER'S THESIS

AUTHOR Bc. Josef Samek

BRNO 2016

BRNO UNIVERSITY OF TECHNOLOGY
VYSOKÉ UČENÍ TECHNICKÉ V BRNĚ

FACULTY OF ELECTRICAL ENGINEERING AND COMMUNICATION
FAKULTA ELEKTROTECHNIKY
A KOMUNIKAČNÍCH TECHNOLOGIÍ

DEPARTMENT OF POWER ELECTRICAL AND ELECTRONIC ENGINEERING
ÚSTAV VÝKONOVÉ ELEKTROTECHNIKY A ELEKTRONIKY

OPTIMAL FILL FACTOR OF SLOT WITH RESPECT OF USED INSULATION OF MOTOR AND DUTY
OPTIMÁLNÍ PLNĚNÍ DRÁŽKY S OHLEDEM NA POUŽITOU IZOLACI MOTORU A PRACOVNÍHO ZATÍŽENÍ

MASTER'S THESIS
DIPLOMOVÁ PRÁCE

AUTHOR — **Bc. Josef Samek**
AUTOR PRÁCE

SUPERVISOR — **Ing. Rostislav Huzlík, Ph.D.**
VEDOUCÍ PRÁCE

BRNO 2016

BRNO UNIVERSITY
OF TECHNOLOGY

Faculty of Electrical Engineering and
Communication

Department of Power Electrical and Electronic
Engineering

Diploma thesis

Master's study field
Power Electrical and Electronic Engineering

Student: Bc. Josef Samek *ID:* 145652
Year of study: 2 *Academic year:* 2015/16

TITLE OF THESIS:

Optimal fill factor of slot with respect of used insulation of motor and duty

INSTRUCTION:

1. Make literature search.
2. Prepare FEM model of electric machine's slot and make analysis of current density in stator slot.
3. Make simulation of temperature distribution in slot to verify influence of current density distribution on temperature in slot.

REFERENCE:

[1] J. Pyrhonen, T. Jokinen, and V. Hrabovcova, Design of Rotating Electrical Machines. Chichester, UK: John Wiley & Sons, Ltd, 2008.
[2] M. van der Geest, H. Polinder, J. A. Ferreira and D. Zeilstra, "Current Sharing Analysis of Parallel Strands in Low-Voltage High-Speed Machines," in IEEE Transactions on Industrial Electronics, vol. 61, no. 6, pp. 3064-3070, June 2014.
[3] M. Popescu and D. G. Dorrell, "Skin effect and proximity losses in high speed brushless permanent magnet motors," Energy Conversion Congress and Exposition (ECCE), 2013 IEEE, Denver, CO, 2013, pp. 3520-3527.

Assigment deadline: 21. 9. 2015 *Submission deadline:* 8. 8. 2016

Head of thesis: Ing. Rostislav Huzlík, Ph.D.
Consultant:

Ing. Ondřej Vítek, Ph.D.
Subject Council chairman

Abstract

Thesis deals with random wound stator - conductors' distribution in stator slot and its influence on proximity effect (non-uniformity of current distribution) in conductors near air gap. Also circulating currents between parallel strands of winding are assumed, same as influence of rotor permanent magnets magnetic field. Conductor level thermal simulation is conducted according to used insulation system of machine and current distribution. Chapter 1 – 3 deals with theory, subchapter 4.3 investigates thermal properties of used materials for thermal simulations and chapters 4 and 5 presents work itself – simulation of given machine (current distribution in conductors) in Ansys Maxwell and thermal simulation in FEMM and Ansys 16.0.

Keywords

Random wound winding, insulation system, circulating currents, proximity effect, skin effect, finite element method, thermal properties of materials, thermal analysis of PMSM, winding hot spots, heat transfer, Ansys, Maxwell, FEMM, conductor level thermal analysis, conductor level simulation, PMSM machine heat loss distribution.

Bibliografická citace

SAMEK, J. Optimal fill factor of slot with respect of used insulation of motor and duty. Brno University of Technology, Faculty of Electrical Engineering and Communication, 2016. 67 pages. Supervisor Ing. Rostislav Huzlík, Ph.D.

Prohlášení

Prohlašuji, že svou diplomovou práci na téma „Optimal fill factor of slot with respect of used insulation of motor and duty“ jsem vypracoval samostatně pod vedením vedoucího diplomové práce a s použitím odborné literatury a dalších informačních zdrojů, které jsou všechny citovány v práci a uvedeny v seznamu literatury na konci práce.

Jako autor uvedené diplomové práce dále prohlašuji, že v souvislosti s vytvořením této diplomové práce jsem neporušil autorská práva třetích osob, zejména jsem nezasáhl nedovoleným způsobem do cizích autorských práv osobnostních a jsem si plně vědom následků porušení ustanovení § 11 a následujících autorského zákona č. 121/2000 Sb., včetně možných trestněprávních důsledků vyplývajících z ustanovení § 152 trestního zákona č. 140/1961 Sb.

V Brně dne …… Podpis autora ……..

Acknowledgements

"If you want to find the secrets of the universe, think in terms of energy, frequency and vibration." Nikola Tesla

First lines of acknowledgement belongs to my supervisor Ing. Rostislav Huzlík, Ph.D. from Brno University of Technology, I am very grateful for all his patience, problem solving ideas, sharing of his skills in FEM modeling programs and all the time spent with me during our personal consultations in Brno and also skype consultations.

I am also very grateful to Ing. Jiří Kurfürst, Ph.D. for cooperation with industry and finding some time for me always, when I needed. For all support during work and also idea of creation of this task - assignment. During process of working on the thesis, I have learnt a lot.

I have to express gratitude to prof. Ingo Hahn from FAU Erlangen - Nürnberg for accepting me to one semester of studies in the university, for providing the material background and support, for consultation time, his patience and willingness to listen.

Next gratitude lines are heading to Ing. Christoph Hittinger for his time, he spent with me during our consultations in Erlangen. Your ability of deep thinking and passion for understanding of the electro-technical problems was very inspiring. Good luck with your dissertation.

I would like to express many thanks to KAAD organization – Pavel Blažek, Markéta Šmalcová, Alwin Becker, Dorit Raderschatt, Marianne Wend, Markus Leimbach, and Mechthild Habermann. Thank you all students from all around the world attending KAAD Jahresakademie 2016 and KAAD Katholikentag Leipzig 2016. Also many thanks to organizers of these events. I would like express gratitude to KAAD for financial support.

Praise to my classmates in Brno – for support during winter semester especially to Ladislav Karásek and Roman Juchelka. Many thanks to my new friends in Germany first of all to Rahel for warm welcome and acceptance and also for patience during my beginning with the German language.

Many, many, many thanks to my Mum, Dad, brother and whole family. First of all for financial support during my studies. I also received generous support from kitchens of my mum and grandmothers during studies. It was delicious, thank you. I am also very much grateful to my brother and dad for encouragement and engagement in the thesis. Your perspective above the thesis, ideas, willingness to understand, and your support was the most important essence during completion during last days before deadline.

I would like also to thank YOU, you who are reading the acknowledgement lines till the end.

I am particularly grateful for the assistance and lessons given by God during thesis elaboration.

Thank you all!

Namaste.

In Bystřice nad Pernštejnem, 08.08.2016 Signed by Author ……

CONTENT

LIST OF FIGURES

LIST OF TABLES

LIST OF SYMBOLS AND ABBREVIATIONS

$\overrightarrow{q_x}$ - vector of heat flux [W·m^{-2}]

$_{\Delta}P$ - represents amount of heat generated inside machine [W]

$_{\Delta}R$ - change in resistance due to change of temperature [Ω]

$_{\Delta}T$ - difference of temperatures [K]

$_{\Delta}\vartheta$ - represents temperature drop [°C]

B_n - peak value of flux density [T]

P_e – proximity effect losses in conductor [$W \cdot m^{-1}$]

R_0 - resistance in at the beginning temperature [Ω]

R_ϑ - is thermal resistance [K·W^{-1}]

T_0 - temperature of distant surrounding or initial temperature [K]

α_T - temperature coefficient of resistance [K^{-1}]

α_c - heat transfer coefficient [W·m^{-2}·K^{-1}]

α_{nc} - heat transfer coefficient for natural cooling [W·m^{-2}·K^{-1})]

α_r - represents radiative heat transfer coefficient [W·m^{-2}·K^{-1})]

ρ_c - resistivity of conductor [Ω·m]

ω - angular velocity of flux density [rad·s^{-1}]

ΔP - is heat flow [W]

AC – alternating current

CD – creeping discharge

CTI – comparative tracking index

dT/dx - temperature gradient in the direction of x axis heat flow [K·m^{-1}]

DVC – dynamic capacitor voltage control

e - Euler's number [-]

FEM – finite element method

GVPI – global vacuum pressure impregnation

J_z – Current density inside conductor [A·m^{-2}]

l - thickness of material [m]

p.u. – proportional units

PD – partial discharge

PE – proximity effect

PWM – pulse width modulation

PMSM – permanent magnet synchronous machine

RPDIV - repetitive partial discharge inception voltage

rpm – revolutions per minute

S - surface of material [m^2]

T – temperature [K]

t – time [s]

THD – total harmonic distortion

THD – total harmonic distortion

ε - emissivity of material [-]

A - assumed area of machine [m^2]

Q – heat [J]

c - specific heat capacity [$J \cdot kg^{-1} \cdot K^{-1}$]

d – diameter [m]

m – weight [kg]

λ - thermal conductivity of the material [$W \cdot m^{-1} \cdot K^{-1}$]

$\sigma = 5.6703 \cdot 10^{-8}$ - Stephan-Boltzmann constant [$W \cdot m^{-2} \cdot K^{-4}$]

1 INTRODUCTION AND STATE OF ART

1.1 Introduction

At the beginning there was a vision of Nikola Tesla and after work an electric machine was invented. Motors are included in almost all human products and saves time and energy of ordinary people. But sometimes it happens, that motor burns out without any reasonable explanation earlier that its lifetime was expected. There is enormous number of possibilities how it may happen.

1.2 State of Art

The thesis will be investigating one of those hypotheses - current distribution in stator slot. For almost every thermal calculation the current density in cross section of stator is considered to be uniform. But in fact there are occurring some phenomena that make the current distribution non-uniform.

Well known effects like proximity effect, skin-effect, circulating currents in PMSM [1] and slot depth of stator can significantly affect the current distribution. These phenomena are normally taken into account in design of large machines and high speed machines[2], [3]. But no one has considered a connection with failure in ordinary electric motors. Especially low speed motors with high number of poles at stator that are designed without gearbox. These motors are fed by currents of higher frequencies also.

High local current density in conductor placed at top of stator slot could lead to local overheating. It may lead to exceeding the permitted temperature of wire insulation and following premature ageing of insulation [4]. Of course premature ageing is very dependent on used materials [5].

Confirmation of this hypothesis would change design process of electric motors and increased reliability and lifetime of designed machines.

2 INSULATION

Insulation materials are used for electrical separation of parts in machine on different electric potential. In general we have gas insulations, liquid insulations and solid insulations. Commonly used in low voltage machines are solid insulations [4].

Solid insulators inside a machine are improving mechanical properties and provide protection of winding against ambient stress. They are also conducting heat away from copper wires to the surrounding of winding.

Ideal insulator has zero conductivity or in other words its resistance is approaching the limit of infinity. Real insulators are always slightly conductive. It makes them impermanent and creates way for degradation of material. All kinds of stresses are described in details in chapter 2.3. Special attention should be given to partial discharge (PD) phenomenon and also creeping discharge phenomenon (CD). PD started to be widely investigated also in low voltage machines as a result of PWM usage [6].

2.1 Insulation in random-wound stators

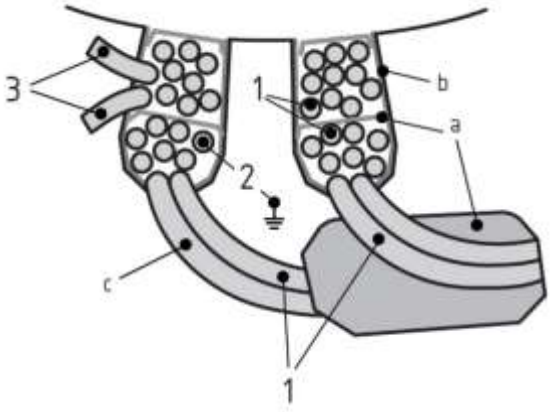

Figure 1. 1 Insulation components of random wound stator [6]

The insulation systems around the market for random-wound machines are usually very similar. The insulation system consists of basic parts – as illustrated in Figure 1. 1.

Where

a. points at interphase insulation
b. points at ground-wall insulation
c. points at turn insulation or in other words strand insulation

And numbers represents following voltages:

1 = phase – phase voltage
2 = phase – ground voltage
3 = inter-turn voltage

Main features of these parts will be described in subchapters. Although every company uses similar parts and materials, the manufacturing process is slightly different in every company according to the coiling and insertion of winding to stator slots.

2.1.1 Basecoats and overcoats of copper wire

Commonly used shape of conductor in random wound stators is round copper wire. Around the wire we bond one or more layers of insulation material. The first layer attached to the copper is basecoat. The other layers are called overcoats. Enameled copper wire can have even more than four layers of insulation depending on intended use [7]. But on wires usually used nowadays in the industry we can find only one or two layers.

Insulation materials are offered in many variations of polyurethane, polyester, polyester-imide and polyimide. Commonly used variants are polyamide-imide insulation resistant to temperatures up to 220 °C, without overcoat and polyester basecoat with polyamide-imide overcoat resistant up to 200°C [4]. For higher temperatures reaching 240 °C is possible to use aromatic polyimide coat. The thickness of insulation is usually between 0.01 mm and 0.1 mm according to the wire diameter and insulation material.

New insulations were introduced due to occurrence of PD in low voltage machines fed by PWM inverters. Technology used in large machines was implemented into enamels of copper wires. Coats are now enriched with nanoparticles of mica or metal oxides [4]. This enrichment rapidly increases PD resistance of organic insulations. The nanoparticles are usually applied to the top overcoat layer of insulation. On a market we can find these wires under the name – corona resistant or PD resistant.

2.1.2 Impregnating resin

Impregnating liquids like polyesters or epoxy resins are used for impregnation of winding. There are several reasons for their usage. At first impregnation holds all copper wires tight together and creates strong binding of wires, ground insulation and stator core. So winding can withstand electromagnetic forces. Also abrasion due to vibrations is eliminated.

Second reason for varnishing is elimination of air gaps (bubbles) between insulation of copper wires. An air bubbles between two copper wires are changing distribution of electrical field based on different permittivity of air and impregnating resin. Partial discharges may occur inside the air bubble due to usage of PWM inverter. This phenomenon is closely described in [4]. Low voltage machines that are operated without PWM have lower requirements for quality of impregnation. Other positive effects of impregnation are thermal properties. Varnish supports heat transfer from copper wires to the stator core.

Common application of impregnation is simple drying (pre-heating) and then dipping of the entire stator in bath. Whole stator is immersed inside pool with epoxy resin or varnish and then moved to drying chamber for curing.

For elimination of air bubbles inside impregnation of winding, some companies uses advanced impregnation techniques like global vacuum pressure impregnation (GVPI)[4][5]. This technology is more expensive due to vacuum technology and has also higher requirements on low viscosity of polyesters or epoxy resins. During this method stator is vacuum dried and then flooded with low

viscosity polyester. These resins are solvent-less to prevent creation of bubbles as a result of solvent evaporation. Resin is pressurized by inert gas to flood every possible gap. Finally the stator is placed to ordinary "oven" to cure and dry the resin [4].

2.1.3 Ground wall insulation

The ground wall insulation is inserted into stator slot before insertion of winding. Phase insulation is thinner than ground wall insulation but is being made from the same materials. Phase insulation is used to separate coils of different phases inside one stator slot.

Mostly used phase to phase and ground wall insulations are "papers" made from synthetic – plastic - materials. These papers are usually made of two or three layers of material. According to required insulation thermal class, different materials and their combinations are used. Thickness of insulation papers is between 0.1 mm and 0.5 mm [5] depending on required dielectric strength.

Dominant patent owner at this field of chemical manufacturing and polymer processing is American company DuPont®. They are owner of patents for commonly used ground wall insulation materials like Dacron™ - polyester fiber, Mylar™ - polyethylene terephthalate films, Nomex™ - meta-aramid material and Kapton™ - polyimide film.

According to [4] new trend at form wound machines is reduction of ground wall thermal impedance. Hopefully this trend may also find its way to the design of low voltage random wound machines. More about ground-wall insulation thermal properties in chapter 4.3.3.

2.2 Quality of insulation

Nowadays customers are expecting high reliability and lifetime of purchased machines and also low price of machines. But these are unnatural antithesis. The expected insulation lifetime before rewinding of a machine is between 20 and 40 years for standard industrial use. This unwritten standard has been created in past [4], before PWM inverter fed machines has appeared on the market. On the other hand we may expect lifetime of insulation in traction applications just longer than 5 years [4]. Sometimes failures and burnouts may occur even in shorter period of time.

In past insulations were dimensioned to prevent premature ageing of insulation with large safety margins. Also current density used to be chosen lower than at present. That led to lower temperatures in machines and very slow degradation of insulations. As a proof of this statement, we can find even these days some large machines from the first half of the 1900s still operating [4].

Due to material development and design progressions we reduced used amount of insulation. New materials have better thermal and also electrical properties. These days we obtain better insulation characteristics from thinner insulations. Also the lifetime of insulation in grid powered machines has increased.

Usage of PWM inverters caused different type of stress to the insulation. As a result of this trend applied stresses to the insulation, like thermal and electrical, were increased. So nowadays we have perfect insulation materials, but under serious amount of stress. And this leads in some cases to premature failure of a machine [8].

2.2.1 Insulation thermal classes

Basic classification of insulations is possible to make according to maximal allowed operating temperature. In the past for every thermal class there was specific letter of alphabet and maximum allowed hot spot temperature. This method of labeling ended at H thermal class insulation. Ever since we use just temperature for intended class, e.g. “Class 220” [4].

Overview of thermal classes used these days, we can find in Table 1. Commonly used thermal classes are F and H, where F class is used at the majority of machines because of the price. H class is less common but is used also these days. Higher thermal classes are used only for special applications. The most important information is hot spot allowed temperature which may occur at some spots on winding due to current imbalance.

Table 1- Thermal classes of insulating materials [5]

Thermal class	Previous designation	Hot spot allowance/°C	Permitted design temperature rise/K, when the ambient temperature is 40 °C	Permitted average winding temperature determined by resistance measurement/°C
90	Y	90		
105	A	105	60	
120	E	120	75	
130	B	130	80	120
155	F	155	100	140
180	H	180	125	165
200		200		
220		220		
250		250		

2.2.2 Dimensioning of insulation

List of stresses the insulation is exposed during lifetime and dimensioning for the stress is called insulation coordination [5].

According to [4] inter-turn insulation is supposed to endure phase to phase voltage. Its maximum value is usually 690 V. Stators designed for higher voltage than 250 V are equipped with ground wall insulation and also insulation separating coils of different phases. We have to also mention that ground wall and inter-phase insulation has lower requirements for thermal properties than coats of copper wire. On the other hand slot insulation must have perfect mechanical resistance because of contact with sharp edges of stator sheets during manufacturing process. We should also count with bubbles in impregnation of winding, while dimensioning the insulation of machine. But no specified advices were given.

After inspection of catalogs of manufacturers there are no doubts that dielectric strength is far behind requirements of [4] Ground-wall insulations from Nomex™, Kapton™ or their combination are able to withstand voltage greater than 6 kV. This dielectric strength was read from the thinnest insulation. Also copper wire manufacturers guarantee breakdown voltage about 4.5 kV.

Inspecting another source [8] brings exact advices given for dimensioning changes of insulation for PWM inverter fed machines. Author speaks that dimensioning is suppressing side effects of switch-on voltage peaks (dV/dt) created by inverters. New inverters generation with soft switching mode are emphasized. The exact design changes are:

- Insulation reinforcement or application of corona resistant insulation
- Insulation reinforcement of first winding coil – respecting of voltage distribution through winding coils
- Application of non-conducting bandages
- Application of semiconducting impregnation resins – reduction of creeping and glowing discharges
- Winding wound with higher number of parallel strands – reduction of proximity effect

Cited paragraph below from [7] page 10, exactly grasps whole dimensioning of insulation:

"A key point to make is that motors which were originally designed and manufactured to operate on sinewave 60 Hz power, are subjected to a significantly reduced dielectric life, when PWM voltage is applied: that is, a motor operating on sinewave power has a longer winding life expectancy than an identical motor operating on a PWM supply, if all the other stresses are constant."

2.3 Premature breakdown of insulation

Breakdown of insulation is complex problem where many factors should be taken into account. The breakdown its self is time dependent process of long degradation of insulation material. There are some places in every winding, where the amount of stress of exact type is higher than in the rest parts of winding.

The developers of PWM inverters are due to efficiency race reducing switching time and losses of power transistors. This leads to the rise of dV/dt during switching time and leads to rise of the stress applied to the insulation.

According to [7] there are several basic mechanism associated with degradation of insulation and premature failure of machine:

- Partial discharge activities due to voltage overshoots
- Dielectric heating
- Growth of material micro cavities due to high frequency stress at power frequency dimensioned insulation
- Space charge accumulation in the enamel of copper wire due to high leading edge voltage (dV/dt) and switching frequency

2.3.1 Thermal stress

Greatest thermal stress source inside of a machine are copper wires. Heat causes slow degradation of insulation materials due to oxidation, pyrolysis and evaporation of molecular substances [8]. While PWM inverter is used there will occur additional heat sources like partial discharge, creeping discharge and dielectric losses.

Dielectric losses inside insulation come from changes of electric field. Dielectric losses energy is converted to heat and causes another heat source at the machine. According to [6] at conventional frequency dielectric losses are very minor. However if we use PWM inverter, the applied frequency increases.

Dielectric losses are increasing with square of frequency [8]. Not only switching frequency of inverter causes dielectric heating, but also voltage over-shots which are carried by far higher frequency of the impulses and their resonance effect [9]. Consequences are at first faster degradation - aging of insulation. And creation of another heat source inside machine that causes rising temperature of winding compared with grid powered machine. This claim supports also [10].

3 CURRENT IMBALANCE

Current imbalance occurs in stator coils for many reasons. In the past it was usually taken under consideration only in large machines (e.g. hydro-generators). Since application of inverters and high speed motors, the knowledge about large machines started to be applied in low voltage machines.

Current imbalance in stator is usually considered with high-speed machines [3], [11]–[13], [2], [14]–[16], where high frequency of AC current creates a current displacement in conductor and also affects nearby conductors. These effects may lead to creation of local hot-spots at winding. We sometimes also use currents of higher frequencies in high torque machines with high number of poles. This brings us very power-full torque and good rpm but may also lead to creation of hot-spots.

In this chapter there will be examined all possible known effects that are influencing imbalance of current - in one single conductor, in parallel strands of coil and between coils of stator winding.

3.1 Skin effect

An alternating current creates non-uniform distribution of current density in cross section of conductor. The current has tendency to concentrate near the surface of conductor. With rising depth of conductor, the current density is lowering. If the frequency of AC is very high, the current occurs only in a very thin layer above the surface of conductor. This phenomenon is known as skin effect.

If we originate from Maxwell's equations, it is possible to analyze the phenomena and describe in analytical formulas same as in [17] at chapter 20. For simplicity there will be the phenomena only in words described and final equations described.

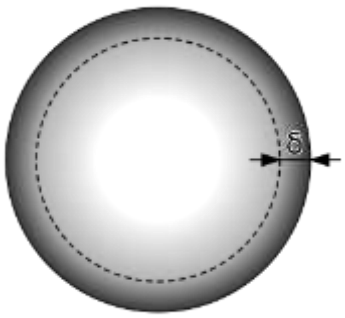

Figure 2. 1 X-Y plane of conductor with skin effect [18]

At first we assume homogenous round conductor same as in Figure 2. 1 in x-y plane. On z axis we can find current density vector **J** [A·m^{-2}], which is on Figure 2. 1 represented by colors: black – maximum current density and white – minimum current density. There is also drawn skin depth – δ. This term will be explained a few paragraphs lower.

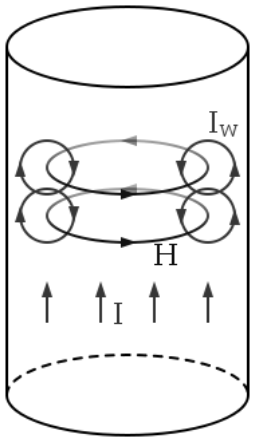

Figure 2. 2 Cause of skin effect[19]

According to Ampere's law alternating current **I** creates alternating magnetic field **H** around the conductor and also inside the conductor. When the intensity of AC changes the magnetic field also changes. According to Faraday's law the change of magnetic field will create counter-electromotive force represented by eddy-currents $\mathbf{I_w}$. Eddy currents are counter-reacting the main current **I**, as we can see in the Figure 2. 2. This leads to current density displacement, exactly to shifting of current from the center of conductor to the surface.

As mentioned in [17], after expression of Maxwell's equations, we obtain analytical expression (3.1 – 1) for the size of current density vector - **J** at any point of conductor.

$$J = J_S \cdot e^{-\frac{d}{\delta}} \tag{3.1 – 1}$$

Where

d [m] is depth of the conductor

J_z [$A \cdot m^{-2}$] is the size of current density vector at the surface of conductor

δ [m] is skin depth or depth penetration

e [-] is Euler's number

Skin depth δ [m] is defined as depth where J_s drops to 1/e (ca. 0.37) of its value. According to [20] page 160, we assume that copper wires are good conductors, so we can use following analytical formula (3.1 – 2) for skin depth calculation.

$$\delta = \sqrt{\frac{2}{\omega \sigma \mu}} \tag{3.1 – 2}$$

Where

ω [$rad \cdot s^{-1}$] is angular frequency

σ [$S \cdot m^{-1}$] is conductivity of conductor

μ [$H \cdot m^{-1}$] is the multiple of vacuum permeability and relative permeability of material

With increasing depth d of a conductor, current density **J** changes its amplitude and also its phase. So at specific distance from the surface of conductor (depth of change - d_c [m]) we obtain current density vector **J** pointing to the opposite direction than the current flowing near the surface of the conductor. The depth of change can be easily calculated by following analytical formula mentioned in (3.1 – 3). Where n represents any positive integer excluding zero.

$$d_c = n \cdot \pi \cdot \delta \qquad (3.1 - 3)$$

This effect we can see in *Figure 2. 3* where y axis represents depth of conductor d and z axis determines current density at the surface. There are also indicated depths of change.

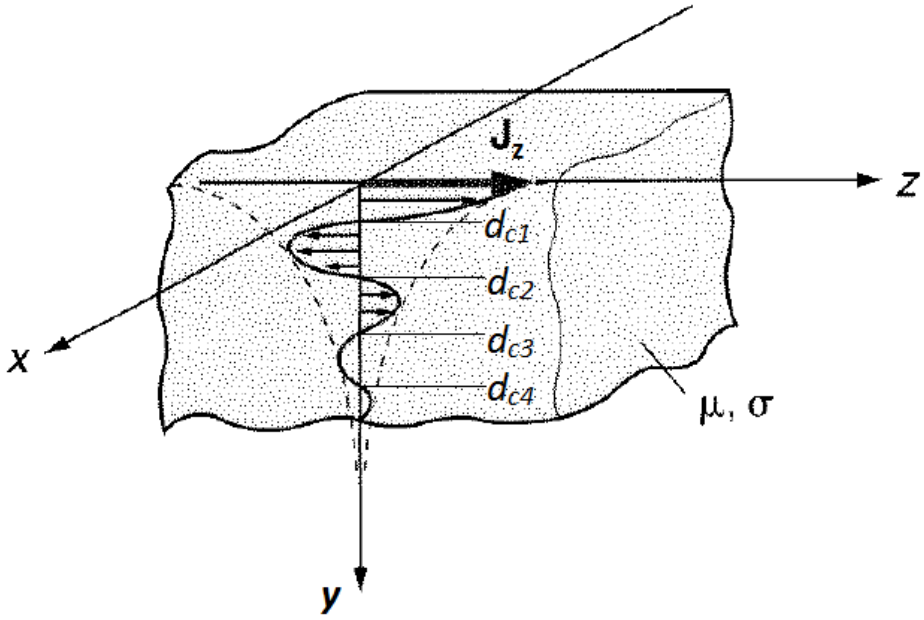

Figure 2. 3 Homogenous conducotor at xyz plane with current density vector ***Jz*** *illustrated*[17]

According to [18] simulations admit that combination of skin effect and proximity effect can lead to occurrence of current density vector oriented against main current flow. The simulations were made for ordinary traction motor fed by PWM not at high frequency. In other words, we may face problem with current flowing in opposite direction inside the conductor. The main condition for appearance of this effect is sufficiently high frequency.

Skin effect is possible to eliminate by using more parallel strands of winding with smaller diameter conductors [8][13].

3.2 Proximity effect

The easiest example is that we have two nearby conductors. The conductors are carrying AC. According to Maxwell's law the magnetic fields of both conductors will intersect the other conductor and inside the conductor there will be induced eddy currents. If we have more conductors, each one will affect all other conductors.

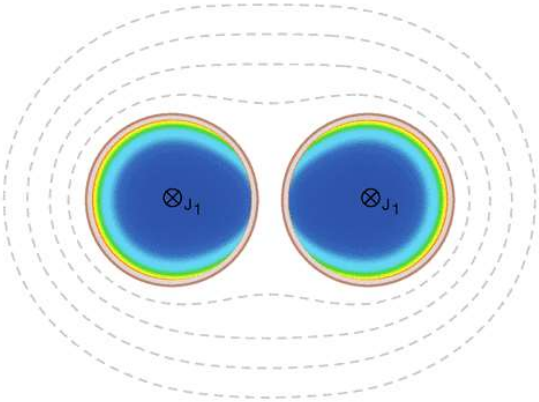

Figure 2. 4 Proximity effect at two nearby conductors[21]

We will obtain inside conductors some areas with higher current density and other areas with lower current density. This phenomena is called proximity effect, it is illustrated in the Figure *2. 4* where dark blue color indicates areas with lower current density and red color indicates area with higher current density. Around conductors are illustrated flux lines.

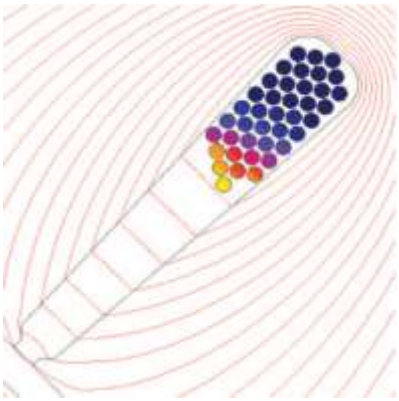

Figure 2. 5 Proximity effect at conductors inside stator slot and slot leakage flux lines[11]

The flux density around conductors changes when we place them inside stator slot. The main problem creates different relative permeability of stator sheets and stator slot. As flux lines are showing in the Figure 2. 5. The phenomenon is called stator leakage flux. This flux changes the distribution of current inside conductors.

The conductors inside bottom part of stator slot keeps the current density uniform (blue color) but at the top of the slot we obtain higher current density (red and yellow). If the stator slot will be filled to the tips of stator tooth, we will obtain the highest current density at the slot opening point.

Study [16] has shown that in their exact case the influence of proximity effect on current imbalance was greater than circulating currents imbalance. Literature [16], [2] states, that very close to the slot opening high leakage flux exists. This linkage flux causes strong proximity effect in the area [12]. According to [14] thick conductors lead to higher eddy current and proximity effect losses. Another study [2] refers that current imbalance at the top of stator tooth appears across speed range of machines so we should not consider this problem only at high speed machines.

As mentioned also in [13], magnetic field near the air gap of stator tooth inside stator slot produces local strong proximity effect and can cause local rising of AC copper resistance that can

lead to serious current displacement in the conductor and increased generation of heat. This effect leads to creation of hot spots on winding [3], [2][25]. These areas should never exceed maximal hot spot allowed temperature listed in chapter 2.2.1, Table 1. This could lead to premature aging of insulation and its breakdown. But this is only one of many phenomenon that may lead to premature breakdown.

In [12] there was suggested analytical formula for calculation of proximity effect losses (see equation (3.2– 1). But in this formula there is not assumed reverse redistribution effect on the field distribution.

$$P_e = \frac{\pi \cdot d^4 \cdot \omega^2 \cdot B_n^2}{128 \cdot \rho_c} \qquad (3.2– 1)$$

Where d[m] is diameter of conductor, ρ_c[Ω·m] is resistivity of conductor, B_n [T]and ω [rad·s^{-1}] are peak value and angular velocity of flux density. So in general the formula of proximity effect P_e[W·m^{-1}] says that proximity effect losses depends on copper area, frequency of electrical current and flux density inside stator slot [18].

Literature [13] states, that proximity effect can be mitigated by transposing conductor strands. In conclusion it is also mentioned that proximity losses are higher in active length of conductors than in end winding. Different arrangement of conductors in stator slot and changes in space between conductors can change current distribution inside the stator slot. It will lead to minimizing the skin effect and proximity effect.

Another source [16] advises different techniques for proximity effect reduction:

- lower PWM current frequency
- change of stator tooth-tip shape
- partial slot filling
- design of winding with litz-wire (twisted wire)

Best literature to get into proximity effect problem in top part of winding is [18], where are very clear results, what proximity effect does. Work includes also thermal simulation, authors aimed for hot-spot areas on winding.

3.2.1 Parallel strands and proximity effect

Position of conductors inside every slot is very important to distribution of current. There were conducted many studies [21] - [27] comparing different winding setup for high speed machines. Due to high frequency of current almost every author compares AC to DC resistivity of wires. The resistivity changes due to proximity effect near stator slot tooth tips.

Different arrangement of conductors inside slot plays a role [3] same as every different winding arrangement of parallel strands in hand and turns of coils [2]. According to following Figure 2. 6 and Table 2, there was conducted FEM analysis of current distribution. Measurement of currents on real machine shown, that differences 10% are smaller. In summary of model authors states, that field flux can be ignored due to great role of inductance and in consequence of small field flux influence, there are no significant circulating currents.

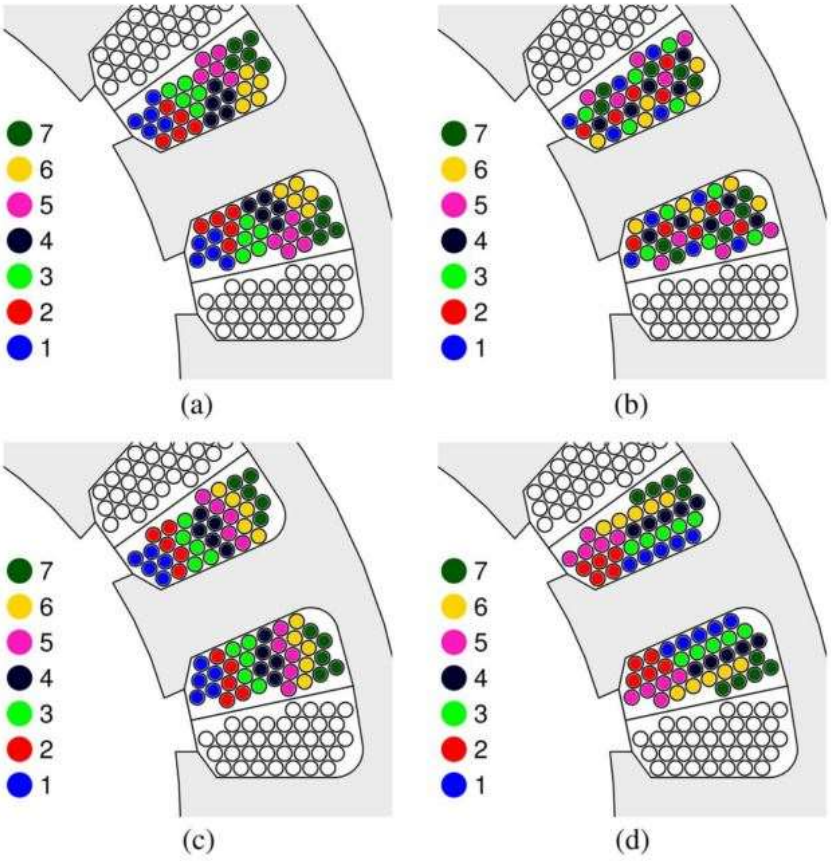

Figure 2. 6 Winding styles for a concentrated fractional pitch winding [3]

(a) Grouped strands, (b) Grouped turns, (c) Radial layers, (d) Tangential layers

Table 2 Transient FEM Results for the Winding Schemes in Figure 2. 6 [3]

Winding style	Strand currents (A)	Total copper losses (W)	Conduction copper losses (W)
Grouped strands	42.5, 11.6, 7.2, 3.6, 2.5, 0.8, 1.2	260	213
Grouped turns	37.1, 15.1, 9.1, 11.7, 9.2, 9.6, 6.8	299	217
Radial layers	35.7, 15.7, 6.7, 1.4, 0.8, 0.6, 1.0	216	167
Tangential layers	7.5, 4.7, 14.3, 36.7, 6.4, 12.6, 5.2	255	196

As we can see in Figure 2. 6, strands close to the slot opening carries significant amount of current. Once more there should be stated, that experimental results shown about 10% lower current difference. In Table 2 the total copper losses includes proximity effect and are taken from FEM

program. Conduction copper losses are calculated from resistances and currents. Authors speaks about possibility of creation of hot-spots on winding, but no thermal analysis was conducted.

So arrangement of conductors inside slot will have an influence on current distribution and consequently to distribution of temperature inside stator slot. There should be pointed, that number of parallel strands also has an effect.

3.3 Permanent magnet - winding eddy currents

While using closed slot design as we can see in Figure 2. 5 or Figure 2. 6, we obtain some leakage flux through stator slot due to closing angle of slot and also slot tooth tips. On the other hand we can use open slot design. This desigh option eliminates the leakage flux.

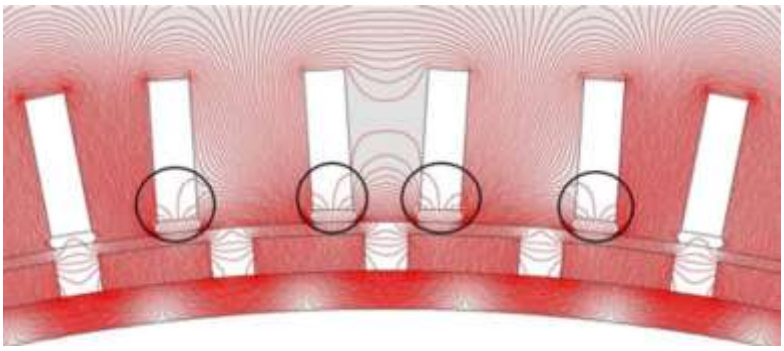

Figure 2. 7 Radial magnetic flux created by rotor magnets[15]

But the problem connected with open slot tooths are eddy currents induced to winding from permanent magnets. As we can see in Figure 2. 7, there is an area inside the slot where the magnetic flux of permanent magnets enters the winding – black circles. Magnetic flux passing through winding induces eddy-currents and creates some additional loses.

This phenomena has been studied in [15] during design process. The flux lines in the Figure 2. 7 are shown at no load operation of designed machine. The flux lines passes through winding, induces eddy currents and increases copper losses at the top of winding. The flux lines of magnets during loaded operation of the machine were not presented.

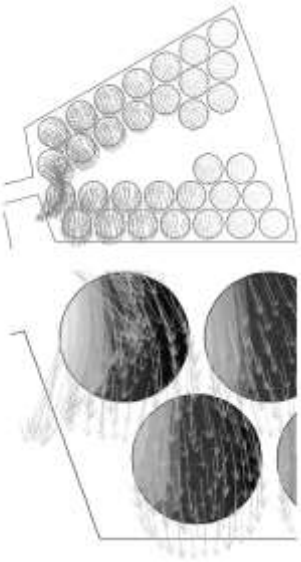

Figure 2. 8 Circulation of magnetic flux in motor winding (short-circuit, 6000rpm) [22]

According to [23] the eddy current losses increase with high frequency harmonics of inverter. The study speaks about creation of hot spots at the top conductor. The thermal analysis refers to reduction of maximum temperature of winding while slot wedges were used.

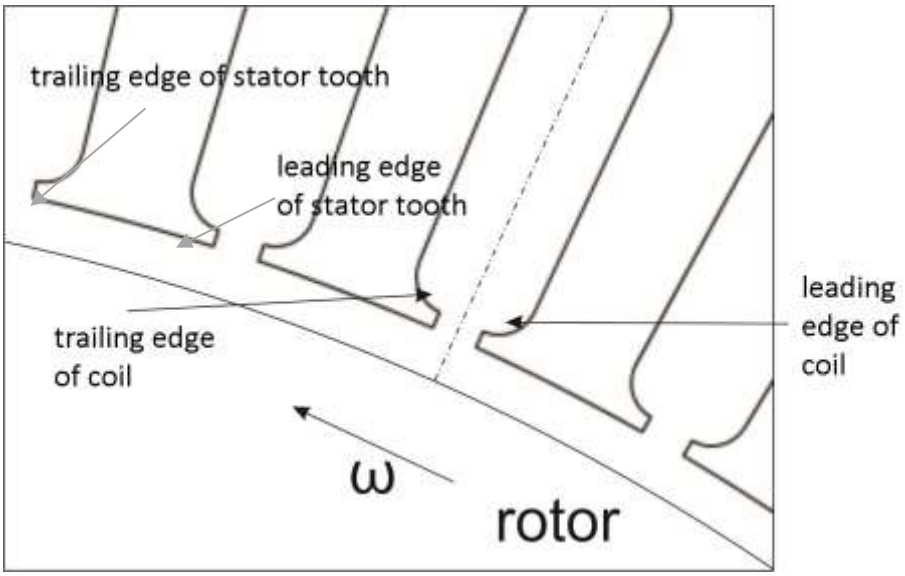

Figure 2. 9 Leading and trailing edge of coil

Also we should assume and consider a leading and a trailing edge of coil side inside stator slot. The leading edge of coil is where rotor magnet is moving towards the stator slot coil. The trailing edge is the area where the rotor magnet leaves the slot last. For easier understanding the situation is illustrated in the

Figure 2. 9. Their study considered proximity effect due to leakage flux as shown in the Figure 2. 5 but also due to radial flux created by rotor magnets passing through stator slot illustrated in the Figure 2. 7.

The radial magnetic flux created by magnets greatly affects the increased losses in the surface conductors of winding. If we compare the simulated AC losses at the leading edge we obtain two

times bigger losses than at the trailing edge of slot opening. According to the authors [22] this higher ac losses can produce localized hot spots leading to the failure. The current imbalance of the leading and trailing edge due to rotor motion were also investigated at [15] so the problem of leading and trailing edge occurs at closed stator slot and also at open stator slot.

3.4 Circulating currents in PMSM

Another problem occurring in stator winding connected with current imbalance are circulating currents. Their appearance is conditioned by occurrence of parallel strands or parallel branches in winding. Also uniform resistivity of every coil cannot be guaranteed by manufacturers. Every manufacturer has its own tolerances at final inspection of machines. This resistance will be different and the results may be different and more significant. Additional problem causes permanent magnets on rotor. The basic scheme showing origin of circulating currents is in following Figure 2. 10.

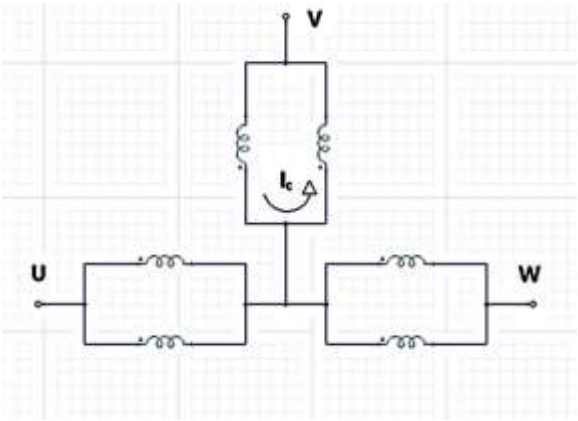

Figure 2. 10 Basic schema of circulating current origin

According to [3] distribution across the parallel strands depends on:

- self and mutual inductances
- strand resistances
- unbalance of linked field flux – magnets, excitation of winding

Linked field flux means in other words the unbalanced electromagnetic pull. Not only stator coils and their manufacturing affect this. We should also consider permanent magnets in open slot stator design.

As [1] states the conductor position inside stator slots are insignificant. Also current imbalance causes significant torque ripple according to winding asymmetries. Circulating currents also increases total machine losses. According to [14] the effect of circulating currents is low according to proximity effect imbalance. At [2] and [3] circulating currents were also simulated but not with consideration of winding impedance imbalance.

Another impact is that circulating currents are causing vibrations of rotor and rotor eccentricity [36]. Circulating currents may lead to local overheating. Particularly when the number of parallel circuit increases and the flux difference in the two coil end parts becomes larger [37]. Splitting coils from single layer to two layers can provide displacement loss reduction. This solution is best

of calculated options. Using of two layer winding increases efficiency and decreases current displacement losses [26].

4 THERMAL MECHANICS

There are two basic areas of thermal mechanics - thermodynamics and thermokinetics.

Thermodynamics observes phenomenon of heat and work and a result of interaction between a system and its surrounding. In thermodynamics we assume steady states at the beginning and end of a thermal event. Thermodynamics works on basis of temperature gradient and temperature balance of system and its surrounding. Every system in nature tries to reach its lowest possible potential.

Thermokinetics is dealing with the heat transfers its self. Under this paragraph, there are three basic mechanisms of heat transfer. This mechanisms will be discussed individually in subchapter 4.1.2.

- Conduction
- Convection
- Radiation

This physics tools will be used in simplified form after acceptance of some restrictive conditions for evaluation of temperature inside winding. This conditions will be listed by every analytical calculation or simulation of the machine. Chapter 4 and subchapters deals only with basic theory.

4.1 Heat and Temperature

There are two basic physics quantities – heat and temperature - that should be explained at the beginning. Heat or in other words thermal energy is inner energy of an object. This energy is total kinetic energy of random motion of all atomic particles inside the object.

$$Q = m \cdot c \cdot {}_{\Delta}T \tag{4.1-1}$$

In equation (4.1-1) letter Q indicates quantity of heat inside an object. Basic unit of heat quantity is Joule [J], m [kg] describes mass of the object, ${}_{\Delta}T$ [K] is difference of temperatures before heat income or outcome and c [J·kg^{-1}·K^{-1}] is specific heat capacity [27].

From electro-technical point of view, we can calculate heat as a “Joule heating” created by current flowing through an electric conductor. This heat is produced by interactions of moving electrons of electric current with static electron shells of atoms. It leads to generation of heat inside every conductor. This heat can be calculated by following formula (4.1-2) called Joule’s law.[28]

$$Q = R \cdot I^2 \cdot t \tag{4.1-2}$$

The other basis physics quantity is temperature. Temperature informs us about absolute thermal state of a mass. If we measure a temperature, it is measured the average kinetics energy of particles inside the mass. When temperature of an object rises, the object receives energy from the surroundings. This phenomena is called heating. Opposite effect is called cooling, the object decreases its temperature and emits the energy to the surroundings.

Temperature is labeled by letter T and the basic unit is 1 Kelvin [K]. The lowest possible temperature is 0 K. This temperature is absolute zero point. We cannot reach this temperature, but it is possible to get very close to this temperature point. According to [29], there are no physical laws that would limit the upper possible temperature.

In 3 dimensional coordinate system, the temperature is function of position and time, as we can see in the equation (4.1-3). This thermal field can be time dependent or time independent – stationary considering the variation of temperature in time.

$$T = f(x, y, z, t) \tag{4.1-3}$$

4.1.1 Temperature scales

Celsius scale

Commonly used temperature scale was created by Andrea Celsius in 1742. It was derived by two points of water. Temperature for freeze of water was set to 0 °C and temperature for boiling of water was set to 100°C. The scale was divided to 100 parts.

Nowadays the Celsius scale is derived in the same way. 0°C is defined as a point created by mixture of chemically pure ice and water at a pressure of 101 325 Pa. 100°C is defined as mixture of chemically pure water and saturated stream at a pressure of 101 325 Pa [28]. Conversion of temperature between scales is given in equation (4.1-4).

$$T_{[°C]} = T_{[K]} - 273{,}15 \tag{4.1-4}$$

Kelvin scale

William Thomson created Kelvin scale. The name of this scale is derived from his rise to the nobility - Lord Kelvin. First point of this scale is 0 K. This point represents the lowest defined temperature. The second point is triple point of water that represents 273,16 [27][29]. Parts of Kelvin and Celsius scales are the same so 1 °C = 1 K.

4.1.2 Fourier's Law

The basic law of heat conduction was established by Fourier in 1822. The law states, that "the heat flux resulting from thermal conduction is proportional to the magnitude of the temperature gradient and opposite to it in sign" [30].

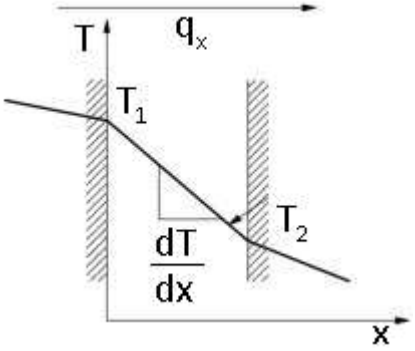

Figure 3. 1 Illustration of Fourier's Law [28]

When this law is expressed by equation (4.1-5) below. For better understanding of basic thermal problem setting and analysis see Figure 3. 1.

$$\overrightarrow{q_x} = -\lambda \cdot \frac{dT}{dx} \tag{4.1-5}$$

Where $\overrightarrow{q_x}$ is vector of heat flux [W·m^{-2}] in positive x direction, λ represents thermal conductivity of the material [W·m^{-1}·K^{-1}] and dT/dx is temperature gradient in the direction of heat flow [K·m^{-1}].

Fourier's equation is valid for gas, solid and liquid materials. According to this law we can also establish thermal conductivity λ of a material. This law calculates with no internal heat generation of material and assumes linear temperature gradient inside material and steady state thermal conduction.

4.1.3 Thermal Conductivity

Thermal conductivity represents ability of a material to conduct heat. This ability is evaluated in term of Fourier's Law. As mentioned above in equation (4.1.2-1) it is denoted by λ and common units are [W·m^{-1}·K^{-1}]. This parameter of a material depend on temperature, pressure and homogeneity of the material.

In [28] chapter 4.2 there was conducted FEM Steady State Thermal simulation of copper plate on elementary example – same as in Figure 3. 1 with $_{\Delta}$T from 20 to 140 K. First simulation was conducted with constant copper thermal conductivity and second simulation was conducted with temperature-dependent thermal conductivity coefficient. The difference $_{\Delta}$Q between simulations was 0.01%. In conclusion of chapter author stathes, that for copper winding inside a machine it is pointless to use temperature-dependent thermal conductivity coefficient, because mistake of simulation method can be much larger.

4.1.4 Specific Heat Capacity

Specific heat capacity is property of matter. This physical quantity says, how much heat we have to add to an object of weight 1 kg from specific material, to rise its temperature for 1 K, as mentioned in equation (4.1-6) where *m* represents mass of matter [kg]. For marking the specific heat capacity we use symbol *c* and commonly used units are [J·kg^{-1}·K^{-1}].

$$c = \frac{Q}{m \cdot {}_{\Delta}T} \tag{4.1-6}$$

The heat is stored in vibration of molecules. It depends on the inner structure of material and degrees of freedom of atoms its structure. The other way of heat storage is in motion of whole molecules inside matter.

There should be also mentioned, that specific heat capacity is temperature dependent. But according to [28] another small simulation experiment, there is negligible influence on thermal simulation of the machine also.

4.1.5 Temperature Coefficient of Resistance

Its symbol is Greek letter α_T [K^{-1}] and temperature coefficient of resistance is usually assumed to be constant for specific temperature range. Usually is this coefficient standardized to temperature of 20 °C [31]. Coefficient is derived in equation (4.1-7) for calculation of resistance change due to temperature change of a material.

$$\alpha_T = \frac{{}_{\Delta}R}{R_0 \cdot {}_{\Delta}T} \tag{4.1-7}$$

Where ${}_{\Delta}R$ means change in resistance due to change of temperature ${}_{\Delta}T$, R_0 indicates resistance at the beginning temperature. Modified equation will be used for evaluation of resistivity of chopper wire inside winding.

Commonly used value for temperature coefficient of resistance for copper 20°C is 0.0039 [K^{-1}]. Literature [32] uses value 0.003862 [K^{-1}].

4.2 Heat Transfer

There are several ways of heat transfer from winding to the surroundings. In future simulations and calculations we will neglect some heat transfer paths of machine. Conduction of heat through shaft will be neglected. We will assume stationary heat source, so we can avoid time difficult transient analysis. Also according to the type of simulation we will neglect end windings and just simulate stator slot. Another assumption is perfect symmetry of machine and heat transfer only in radial direction.

Cooling is mostly done by conduction through stator parts and then by radiation and convection to surrounding area in machines with natural cooling system. We have also machines with active cooling system, mostly is used inner or outer air ventilation [33]. But we can also have water cooling inside of machine.

4.2.1 Conduction

From physical point of view, conduction is propagation of vibrations from one atom to another. During conduction the atoms only change its vibration but stay in their original position. This type of heat transfer is common for solid materials.

Conduction is important inside stator. Due to conduction heat permeates from winding through insulation to stator slot sheets and then heads out of the machine. For conduction literature [33] gives us some basic equations for easy understanding.

For temperature drop ${}_{\Delta}\vartheta$ evaluation in homogenous material we can use:

$${}_{\Delta}\vartheta = \Delta P \cdot R_{\vartheta} = \frac{\Delta P \cdot l}{\lambda \cdot S} \tag{4.2-1}$$

Where

$$\Delta P = \int_S \vec{q} \cdot d\vec{S} = \int_S -\lambda \cdot gradT \cdot d\vec{S} \tag{4.2-2}$$

Equation (4.2-1) represents basic thermal equation, where ${}_{\Delta}\vartheta$ [°C] represents temperature drop, R_{ϑ} [K·W^{-1}] is thermal resistance and ΔP [W] is heat flow. The thermal resistance can be further calculated from l [m] thickness of material, S [m^2] surface of material and λ [W·m^{-1}·K^{-1}] thermal conductivity of material.

In (4.2-2) we further describe heat flow as function of heat $\vec{q}$ [W·m^{-2}] flowing through bounded surface of material, where heat can be expressed from equation (4.1-5).

4.2.2 Convection

Convection is caused by motion of atoms from their original position to another position. This means that the matter must have inside free atoms. During convection the heat is transferred with flow of substance – liquid or gas.

In steady state we can use equation (4.2-3) for evaluation of convection:

$$ {}_{\Delta}P = \alpha_c \cdot A \cdot \Delta T \tag{4.2-3}$$

Where ${}_{\Delta}P$ [W] represents amount of heat generated inside assumed area A [m^2] of machine and α_c[W·m^{-2}·K^{-1}] heat transfer coefficient. Evaluation of heat transfer coefficient is quite challenging problem.

According to the origin of flow, there are two types of convection. First one is natural convection. Created in natural way close to any hot surface. There are factors influencing this convection like shape of the object and temperature of the object. According to literature [33] we can assume heat transfer coefficient for natural convection stated in equation (4.2-4), where α_{nc} [W·m^{-2}·K^{-1}] is heat transfer coefficient for natural cooling.

$$ \alpha_{nc} = 6.5 + 0.05 \cdot \Delta T \tag{4.2-4}$$

Forced convection or in other words heat advection is provided by an object that moves with the fluid. Usually a fan or pump is used. This increases heat exchange a lot. For example fluid radiator systems are sometimes used. Forced convection is far more efficient than natural convection.

4.2.3 Radiation

If we speak about thermal radiation, we speak about electromagnetic radiation of specific wave length. Thermal radiation wave lengths are between 0.1 μm and 100 μm. This range also includes visible light spectrum between 0.4 and 0.8 μm [28]. So most of thermal radiation happens in infrared electromagnetic spectrum.

Every object with higher temperature than 0 K radiates electromagnetic energy to its surrounding and also accepts radiated electromagnetic energy from other objects. This energy is radiated and accepted through surface of the object and defined by Stephan-Boltzmann law. Following equation does not assume back-reflected waves from the surface of machine.

$$ {}_{\Delta}P = \sigma \cdot \varepsilon \cdot A \cdot (T_0^4 - T^4) \tag{4.2-5}$$

Where $\sigma = 5.6703 \cdot 10^{-8}$ [W·m^{-2}·K^{-4}] represents Stephan-Boltzmann constant, T [K] is temperature of surface of the object and T_0 [K] is temperature of distant surrounding and A [m^2] is surface of considered machine that radiates electromagnetic waves.

Emissivity ε [-] is a number between 0 and 1, where 1 is emissivity of ideal black surface at the given temperature. Closely the Black body radiation is described by Stefan-Boltzmann law. Emissivity of every other material is smaller than emissivity of the ideal black surface. For 0 we assume ideally white surface that emits no thermal radiation. Emissivity gives us information about effectiveness of emitting energy in form of radiation form an object.

Emissivity is changing not only with material, the most important is surface finish. For example emissivity of aluminum foil is 0.03 compared with anodized aluminum 0.9 makes a model example [34]. Another example is polished copper – 0.04 and rough copper 0.91. Black paint has emissivity around 0.9 [34].

Objects with lower emissivity than 0.2 are difficult to measure with infrared thermometer because of their high reflectivity [29].

For practical purpose we usually use following equation:

$$_{\Delta}P = \alpha_r \cdot A \cdot {}_{\Delta}T \tag{4.2-6}$$

Where α_r [W·m^{-2}·K^{-1}] represents radiative heat transfer coefficient.

4.3 Thermal properties of materials for simulations

According to given insulation system of the simulated machine H = 180°C (for more see chapter 2.2.1) were found the closest material properties.

4.3.1 Copper

According to [35], thermal conductivity of copper is listed for 380 [W·m^{-1}·K^{-1}] but there was no specified temperature .

Source [36] gave us better answer. According to this study for thermal fusion related materials, for 450 [K] is given thermal conductivity 389.93 [W·m^{-1}·K^{-1}] and specific heat capacity 403 [J·kg^{-1}·K^{-1}].

4.3.2 Sheets, Magnets

According to isovac® data sheet for M470-50A stator and rotor sheets, their material has thermal conductivity 33 [W·m^{-1}·K^{-1}].

For permanent magnets N38UH on rotor was found thermal conductivity 7.6 [W·m^{-1}·K^{-1}] at company list Arnold Magnetic Technologies. Both materials suits to range given in [5].

4.3.3 Ground-wall insulation

Ground-wall insulation thermal conductivity is simple to evaluate. According to this article [37] there are two main variables. First is of course type of material and the second one is density of the material. According to the experiment due to change of ground-wall insulation from Nomex® N_410 with thermal conductivity 0.139 [W·m^{-1}·K^{-1}] to ArPaxX with thermal conductivity 0.25 [W·m^{-1}·K^{-1}], there was increased current in winding and also torque by 5% due to better

thermal properties of insulation [37]. In result the temperatures in winding of machines with both insulations were the same.

Also article [38] reports great improvements of efficiency + 0.7% due to improvement of thermal conductivity of ground-wall insulation. There were also copper loss reduction, winding temperature reduction and iron loss reduction. This effect was obvious on thermal conductivity improvement from 0.16 to 0.308 [$W \cdot m^{-1} \cdot K^{-1}$].

DuPont™ also produces polyimide film ground-wall insulation with better thermal conductivity. Their product [39] has thermal conductivity 0.46 [$W \cdot m^{-1} \cdot K^{-1}$].

So usage of same material with higher density brings us better thermal conductivity. This supports also [40], where different thicknesses of the same material have different thermal conductivities. For our machine according to [40] and insulation thickness was linearly approximated thermal conductivity 0.164 [$W \cdot m^{-1} \cdot K^{-1}$].

4.3.4 Copper wire coating

Copper wire coating used in machine consists of two layers. As basecoat there is used theic polyester and as overcoat there is layer of polyamide imide. Thermal class of copper wire is 200.

Due to very small thickness of copper wire coating we will assume only one layer of coating with worst thermal properties. It is very difficult to obtain precise data for polyamide imide, where many different literature sources defines thermal conductivity between 0.1 – 0.3 [$W \cdot m^{-1} \cdot K^{-1}$]. Higher density of theic-polyester indicates better thermal conductivity, so we will assume only copper wire coating consisted from polyamide imide.

Small thickness of coating wire and information provided in, there was chosen thermal conductivity 0.17 [$W \cdot m^{-1} \cdot K^{-1}$].

4.3.5 Impregnating resin

For impregnation of machine is used Voltatex® resin consisting of unsaturated polyester imide. Thermal conductivity according to technical list is 0.23 [$W \cdot m^{-1} \cdot K^{-1}$] and temperature index of resin is 220°C.

In technical list there was not given specific heat capacity of the material. According to [41] polyimide heat capacity for temperature 177 °C is 2000 [$J \cdot kg^{-1} \cdot K^{-1}$]. Another source [42] measured 1651 [$J \cdot kg^{-1} \cdot K^{-1}$] at temperature 175 °C for a bit different material.

Novel approach to problem of thermal conductivity of impregnating resins has brought idea of enrichment with nanoparticles. If we enrich impregnating resin with nanoparticles the thermal conductivity rises. For example literature [43] states thermal conductivity of resins up to 5 [$W \cdot m^{-1} \cdot K^{-1}$]. That is 20 times more than standard used one resin has. Article [44] states, that without Nano fillers the thermal conductivity is up to 0,3 [$W \cdot m^{-1} \cdot K^{-1}$]. Another approach is usage of silicone resins, they resistance to thermal aging is excellent, but they have low thermal conductivity – around 0.2 [$W \cdot m^{-1} \cdot K^{-1}$].

5 ELECTRO-MAGNETIC SIMULATIONS

Technical documentation of simulated machine was provided by manufacturer. For protection of their know-how, model type and design sheets of existing machine, the results of electrical part in Maxwell – like induced voltage or torque are multiplied by random constant. Percentage comparison with manufacturer's data sheet is not changed. Current, losses and thermal analysis results were not changed. Temperatures of winding from type testing of machine were not provided by manufacturer.

There should be presented two different models built in FEM processing programs. In Ansys Maxwell there are build models of whole machine including all possible losses. On the other hand there was also build simple model in FEMM for verification of results and comparison of these two FEM processing programs.

Both models are built in 2D modelers with setting of model depth equal with stator packet length. According to coil pitch is equal to 1, in every simulation and analytical calculation are neglected end windings. For simulations was chosen temperature 165 °C in winding for calculation of copper resistance according to Table 1 and designed insulation class.

5.1 Ansys MAXWELL – Current Simulation - Nominal power

5.1.1 Parametric model

According to literature search – chapter 3.3 about permanent magnet winding eddy-currents, it was decided to build parametric model of machine for future optimization of stator tooth tip height due to these eddy currents. Documents about parametrization of machine are in Attachment A.

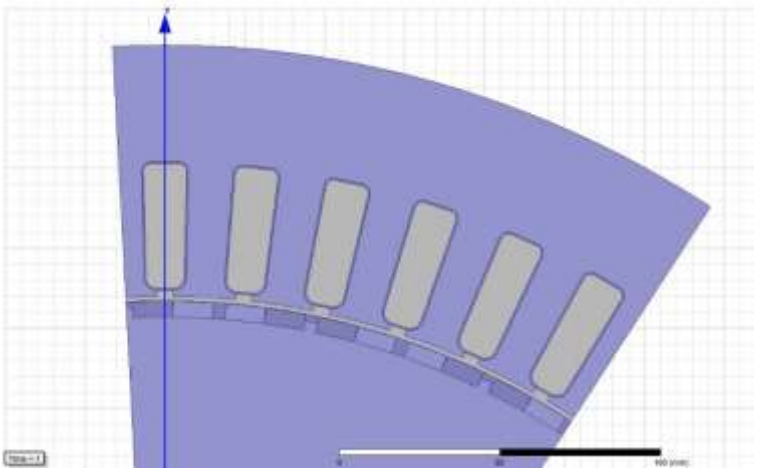

Figure 4. 1 Parametric model of machine scripted in Visual Basic Script

According to the parametrization of model there was build a ·.vbs – Visual Basic Script for Ansys Maxwell for building a parametrical model. In Figure 4. 1, we can see final model of chosen machine including ground-wall insulation.

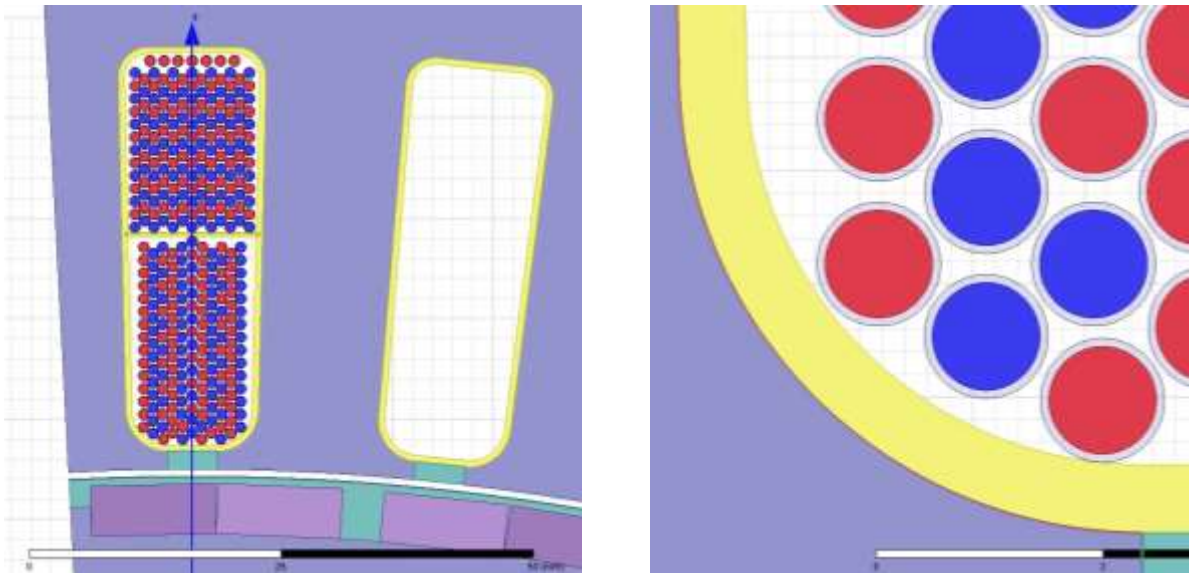

Figure 4. 2 Winding inside stator slot including wire coating insulation

According to diameter of conductors there was build a parametric model that allowed us to change spacing between conductors, diameter of wire and also position of whole winding inside stator slot. Copper wire illustrated in Figure 4. 2 has two color – red and blue. This means the coils are wound from two parallel strands (bifilar winding). Coating of copper wires and ground-wall insulation was suppressed in electro-magnetic models to reduce solution time.

5.1.2 Setup of winding

In random wound machine it is very difficult to simulate distribution of conductors. It is given by manufacturing process. Conductors are wound on winding machine, after that they are being manipulated and transported for inserting to stator slots. During this process the conductors of coil are moving freely in the bound. Due to this random motion of conductor in bound during manufacturing process it is impossible to find any sequence for distribution of them in stator slot. We simulated three possible cases. In compare with Figure 2. 6 simulated machine has only two parallel strands in winding. So we should expect smaller proximity effect and circulating currents.

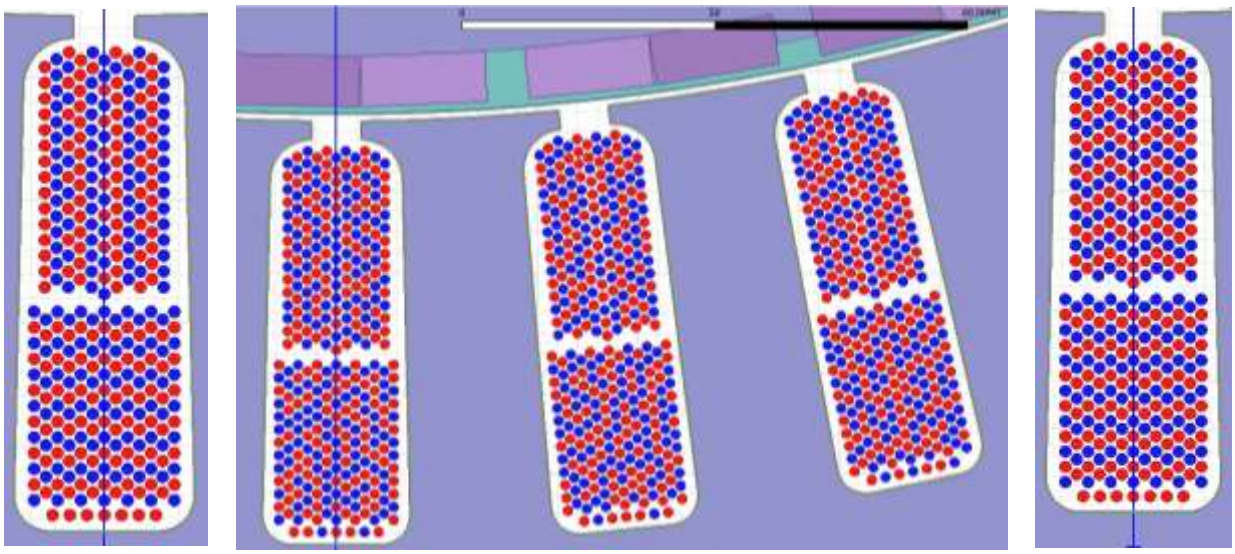

1-Tangential **2-Random** **3-Radial**

Figure 4. 3 Distribution of conductors inside stator slot

In Ansys Maxwell there were built three types of winding setup of two layer winding as we can see in Figure 4. 3. Coils wound form two parallel strands are illustrated by red and blue color. In bottom part of slot – lower layer of winding proximity effect is negligible so conductors for type 1 and 3 are being kept in the same order.

Type 1 has tangential layers in top part of winding and Type 3 has radial layers in top part of slot. For Type 2 we set arrangement of three randomly inserted slots. This basic patterns were used for filling all required stator slots. For nominal load simulations were used voltage excitation sources and for open circuit were used external circuit schematics. In external circuit it is very easy to evaluate circulating currents.

5.1.3 Importing geometry

In this chapter there will be investigated influence of stator sheet holes on Ohmic losses and iron losses. In first model we simulated stator sheet without any holes. This model of stator sheet is similar with Figure 4. 1. The other two models are in figures on next page.

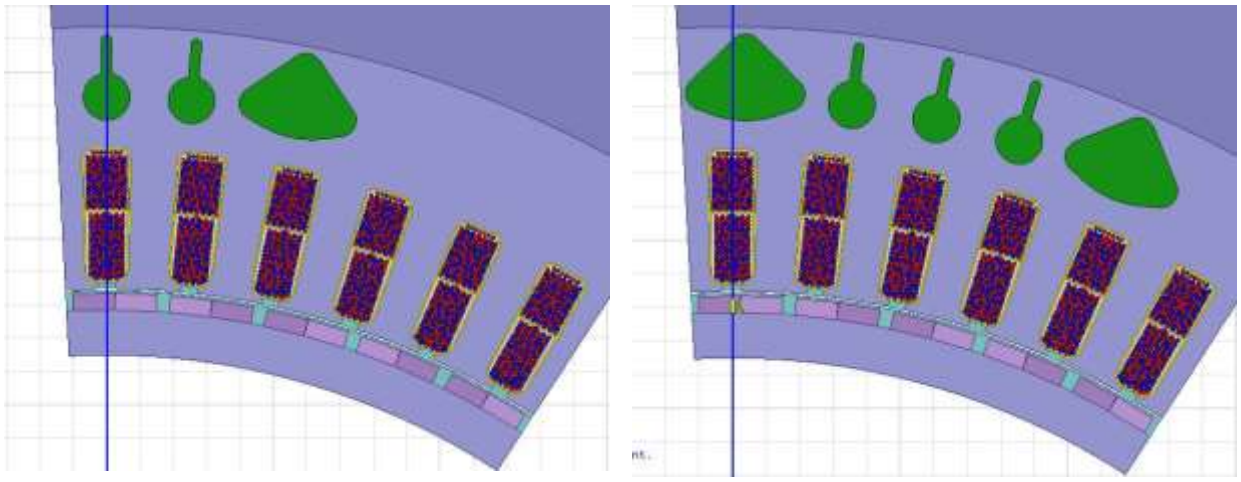

A B

Figure 4. 4 A - Hybrid magnetic circuit type, B – Full magnetic circuit

In Figure 4. 4 A and B there are two types of holes in stator sheet. The problem with setting of holes to model was different symmetry of water cooling system (triangular rounded holes) and symmetry of electrical circuit.

In hybrid magnetic model there is one more round hole due to symmetry of electric model, but the position of water cooling responds almost real machine. On the other hand in full magnetic model there is whole pattern of stator holes, but it repeats more often than in real stator.

The results from Ohmic loss, core loss and current distribution in worst conductor were compared. The results of core losses are listed in following Table 3 influence of magnetic circuit changes was so small, that there was no influence on current distribution or Ohmic losses. Current distribution in worst conductor will be closely described in chapter 5.1.4. Jz in worst conductor was measured as maximum reached value.

In view of the fact that we want to verify possibility of creation of hot spots, it was chosen Hybrid magnetic circuit type - the type of model with greatest RMS value of current in leading edge of coil.

Table 3 Comparison of stator sheets designs

	Core loss [W]
Without holes	400
Hybrid circuit	402
Full magnetic circuit	407

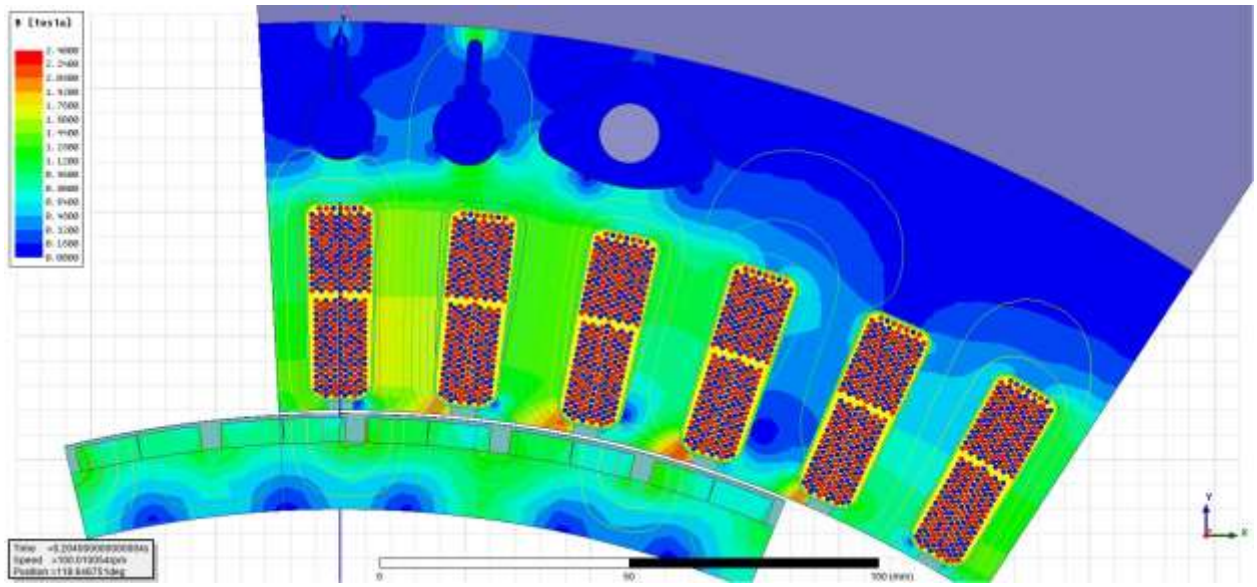

Figure 4. 5 Flux density inside machine including flux lines

Flux lines in *Figure 4. 5* shows that part of magnetic flux flows around second stator hole. I tis main reason for increase of core-losses with imported geometry. In stator tooth the magnetic flux density reaches maximum of 1.71 T. In stator tooth tip we can see effect of leading and trailing edge, where leading edge has higher magnetic flux density and trailing edge has lower magnetic flux density this also affects core losses and we will observe influence of this effect in thermal analysis.

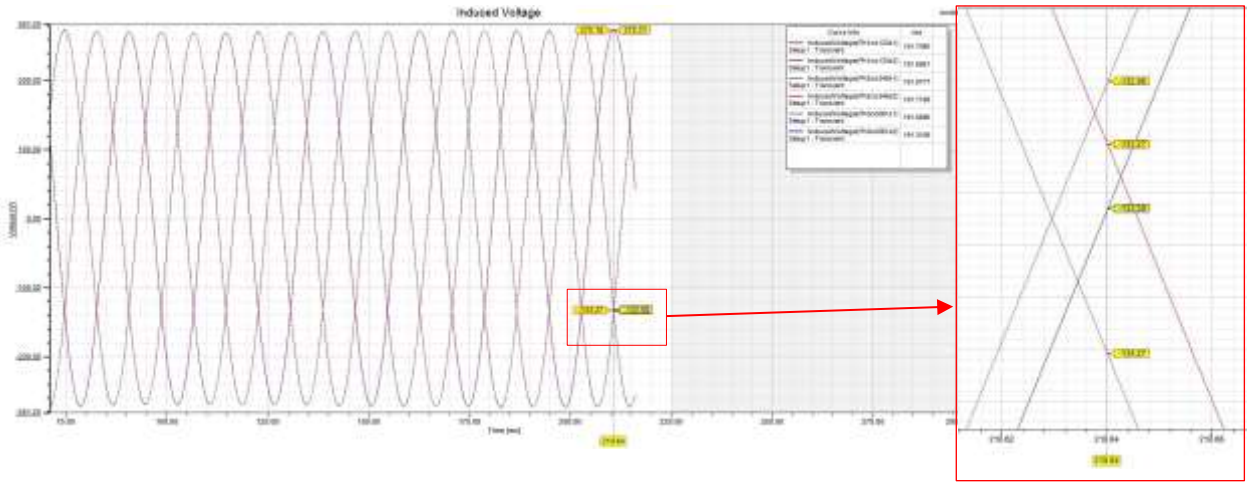

A B

Figure 4. 6 Winding Induced voltage – A whole graph, B – detail of parallel strands difference

First results are typical simulations of machine. We compared simulation with design data sheets of the machine. The induced U-V phase voltage U_i in our model is about 0.6 % deviated from original data sheet value. In Figure 4. 6 there is induced voltage for model 2 – Random distribution of conductors. Other types – 1 and 3 have almost the same results, where the deviation is +/- 0.13 % compared with model 2 – (random arrangement) in different phases of model. As we can see in part B of mentioned figure, there are slight differences in induced voltages between strands of winding.

Nominal torque 48 Nm for model 2 – (Random distribution of conductors) corresponds almost perfectly. Deviation is +/- 1 % from catalog value. Torque results could be more accurate but the solution time of model is already very long. Mechanical transient of motor starting is not completely steady.

5.1.4 Current distribution in models

At first we have to inspect in which place occurs the greatest current imbalance. For easier comparison of results due to opposite current flow it was chosen to compare Ohmic losses at first, so positive and negative current flow is eliminated and reading of results is easier. Following figure was captured in time of maximum phase current.

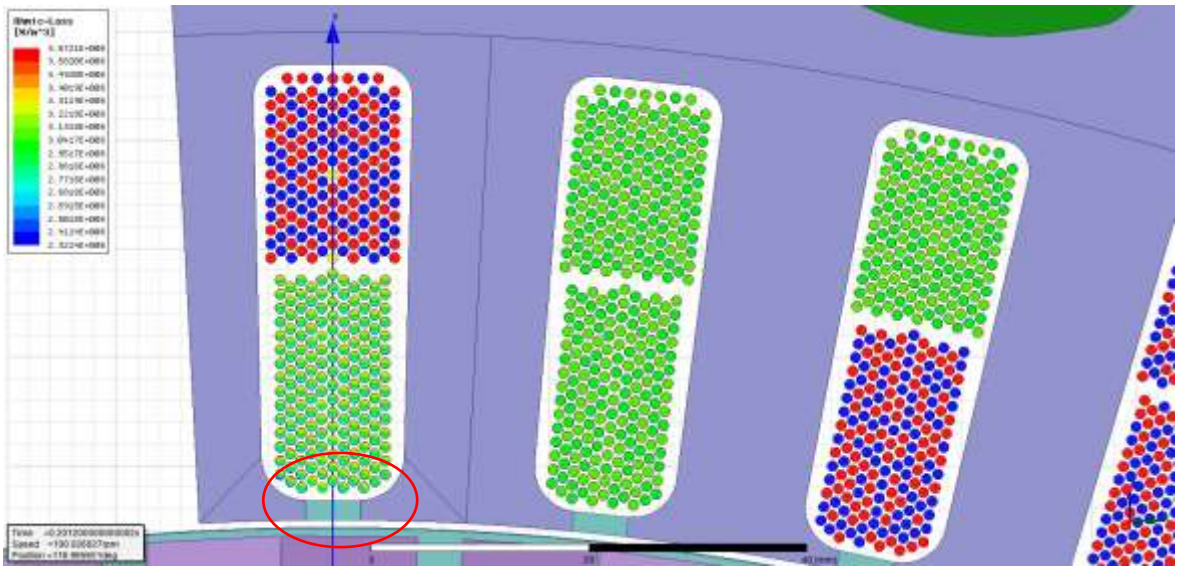

Figure 4. 7 Ohmic Loss in phase U in maximum current of phase

In Figure 4. 7 above, we can see stronger proximity effect in every second stator slot. This effect occurs due to two layers of winding and one step coil pitch. In each second stator slot where bottom coil is from different phase than top coil, there is problem with magnetic flux lines passing through slot. This is possible to see in detail in Figure 4. 13 where amount of flux lines passing through left slot is significantly different in compare with right slot in the figure.

If we inspect current distribution in winding with 1-Tangential, 2-Random and 3-Radial conductors setting, there are no big differences during nominal power operation. Following figures shows current distribution inside conductors of stators slot. Next to J_z – current density plot, there is always stator slot conductors arrangement to compare the influence of conductors' arrangement inside winding on proximity effect.

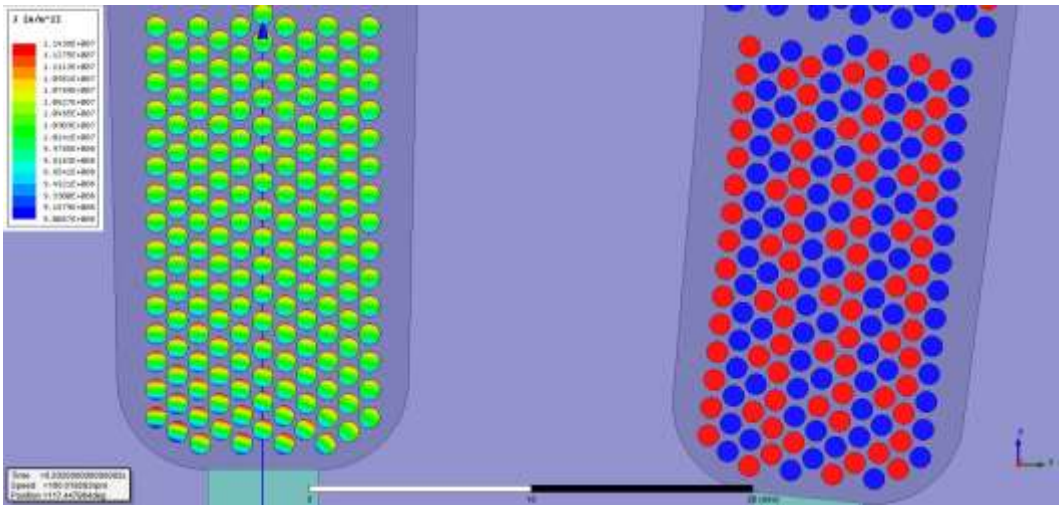

Figure 4. 8 Current density Jz – type 1 – Tangential arrangement of conductors

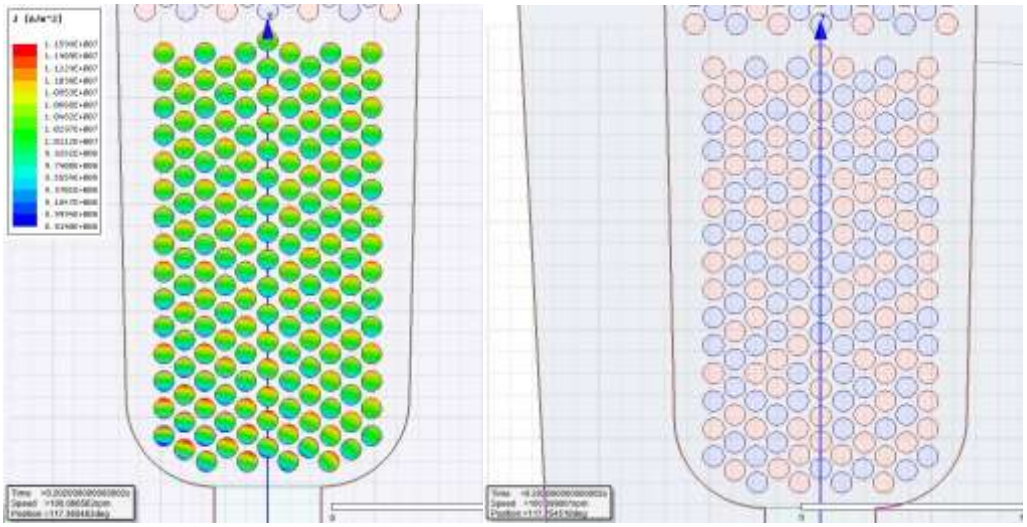

Figure 4. 9 Current density Jz – type 2 – Random arrangement of conductors

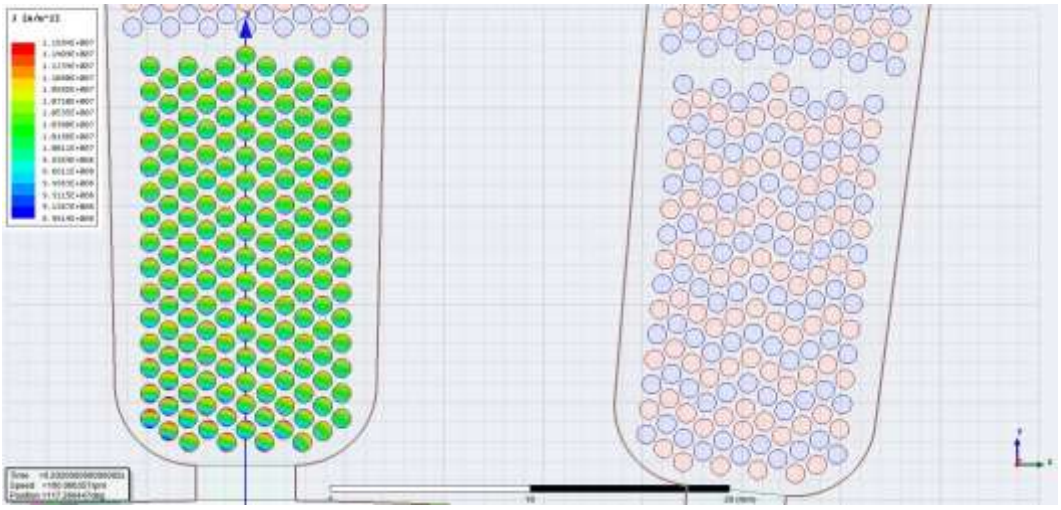

Figure 4. 10 Current density Jz – type 3 – Radial arrangement of conductors

On first sight there are no significant differences between arrangements of conductors in Figures 4. 8 – 4. 10. After closer inspection of conductors' arrangement there are obvious patterns in proximity-effect of parallel strands. Different arrangement creates slightly different proximity effect in trailing edge of coil.

In following Table 4 are listed Ohmic losses in winding including proximity effect. Model types 2 and 3 are corresponding but in model 1 the losses are lower. This could be caused by smaller proximity effect in parallel strands due to tangential arrangement of conductors.

Table 4 Total Ohmic loss comparison across models

Arrangement of conductors	Ohmic loss [W]
Type 1 - Tangential	7147
Type 2 - Random	7357
Type 3 - Radial	7356

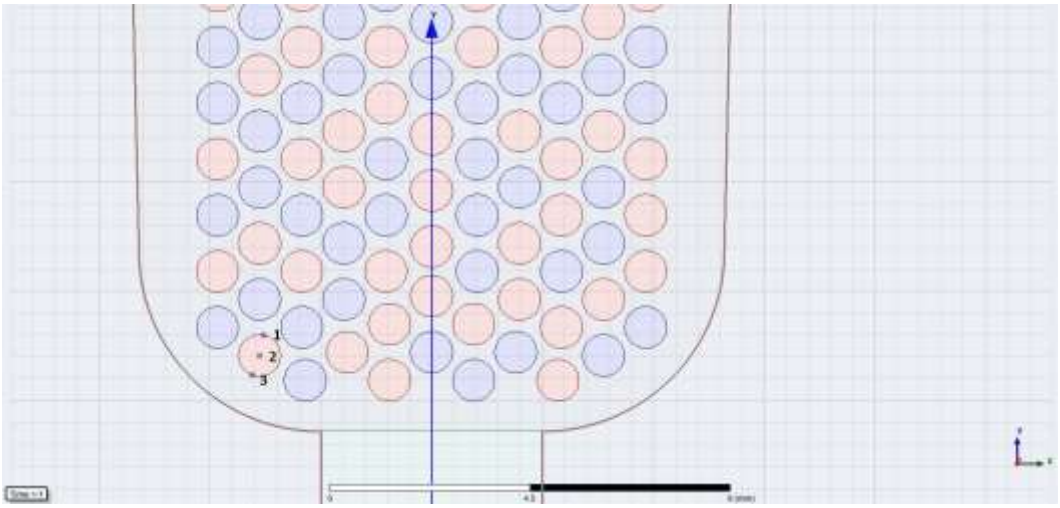

Figure 4. 11 Points in conductor with greatest proximity effect

For deeper investigation it was chosen the random arrangement of conductors. Inside conductor were inserted points 1 – 3 to observe current distribution over time. The points are drawn in Figure 4. 11. From point illustrated above were exported transient waveforms of current density.

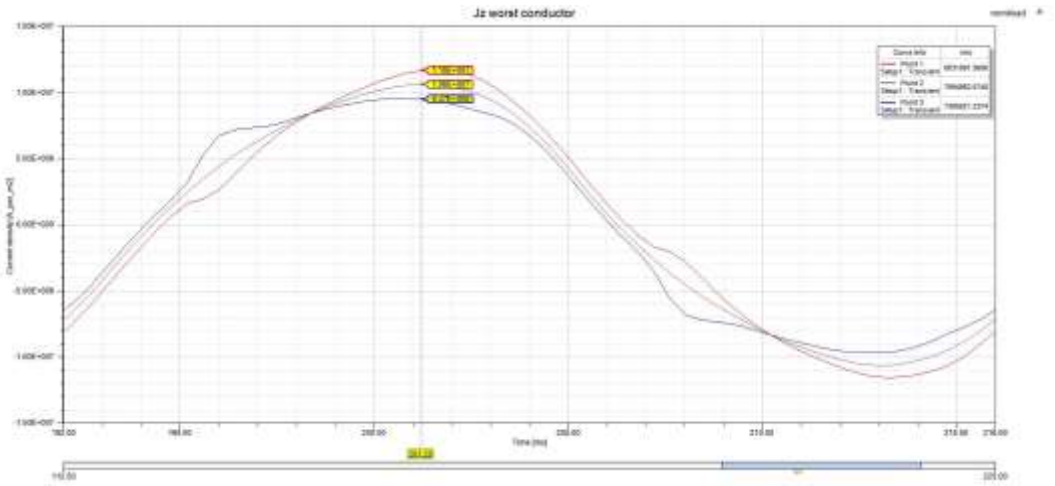

Figure 4. 12 Transient current distribution in conductor – one period

As we can see from Figure 4. 12 there is significant difference in current density in all three selected points due to proximity effect in stator slot. The distortion of sine wave is caused also by change of direction of field flux due to motion of permanent magnets on rotor. The effect of permanent magnets is possible to observe perfectly in Figure 4. 12 at time 195 ms. In the time new permanent magnet enters to the air gap between stator teeth. This is illustrated in Figure 4. 13.

If we compare RMS values the difference is not so great only +5.4 % in point 1 and – 3.8 % in point 3 in comparison with value in middle of the conductor – point 2. For further temperature influence there will be conducted thermal analysis.

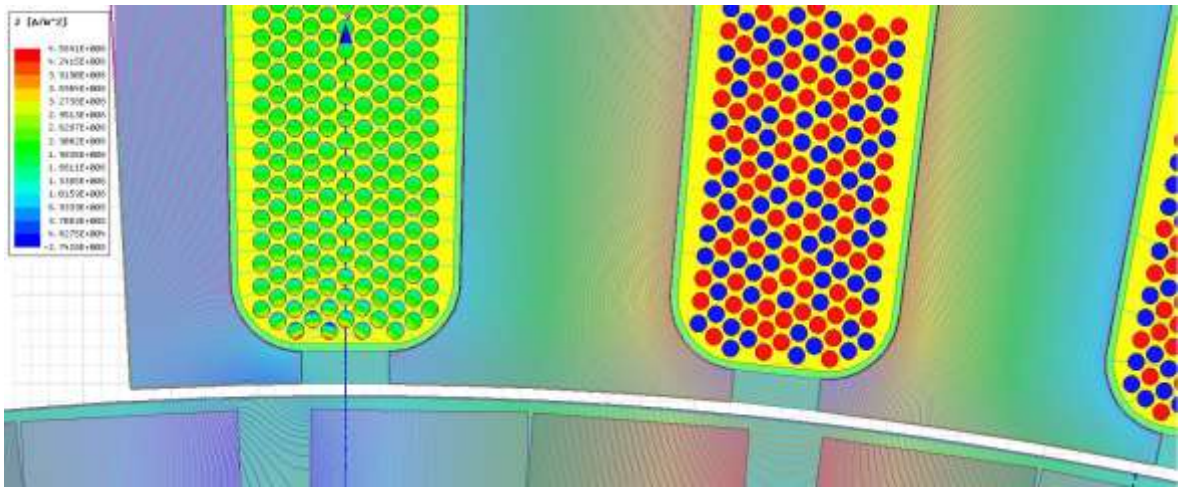

Figure 4. 13 Flux lines and current density Jz in simulation time 195 ms

5.2 Ansys MAXWELL – Current Simulation – Open Circuit (OC)

During open circuit operation we will inspect circulating currents and compare them along the three created models shown in Figure 4. 3. Also eddy currents inside winding could pose a role in heating of conductor during OC operation.

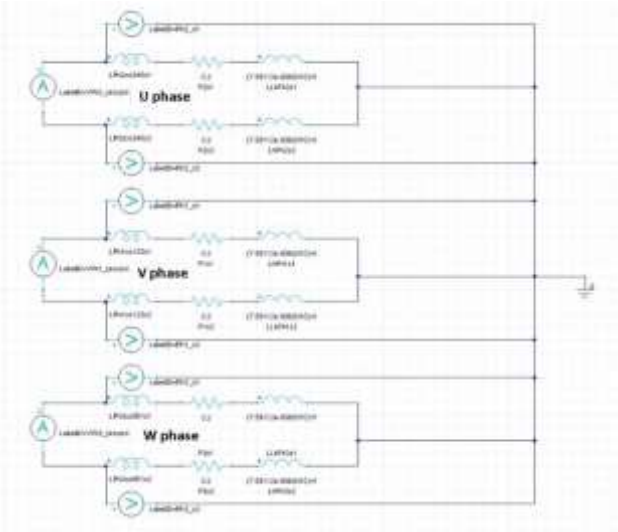

Figure 4. 14 External circuit schematics used for OC model

Schematics illustrated in Figure 4. 14 was created in circuit editor for Maxwell. For better clarity of interpreted results, there will be illustrated circulating current flowing from parallel strands s1 to strand s2. There is also flowing current of opposite sign from strand s2 to strand s1, but these currents were deleted from following graphs. Core losses and copper losses were in all simulated models were equal, so there is no comparison of losses along models.

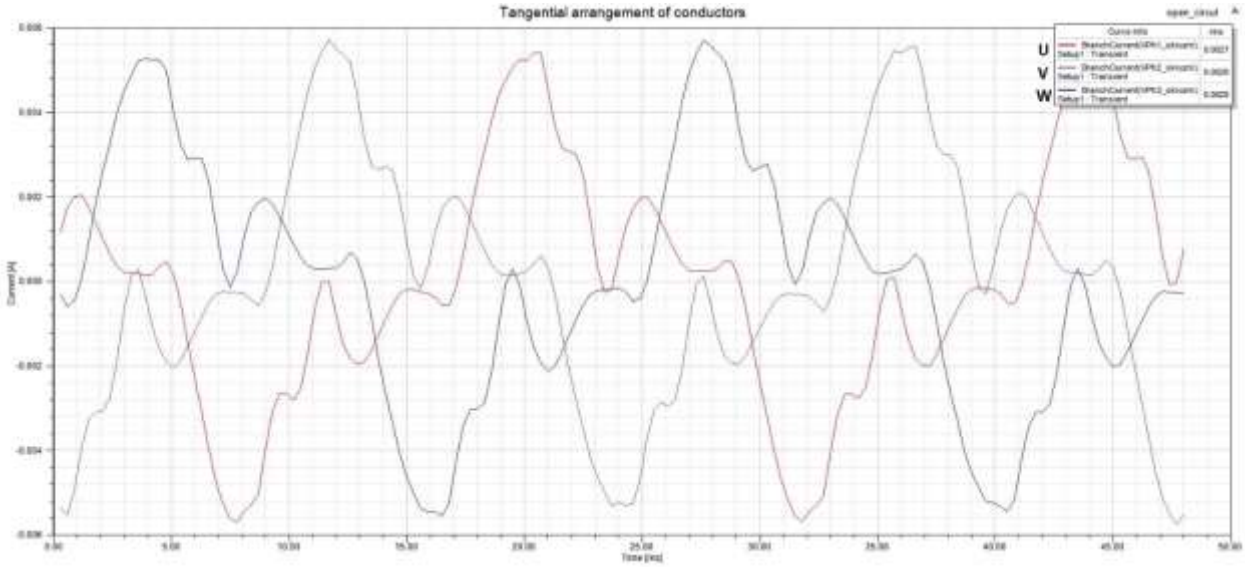

Figure 4. 15 Tangential arrangement of conductors – Circulating currents OC

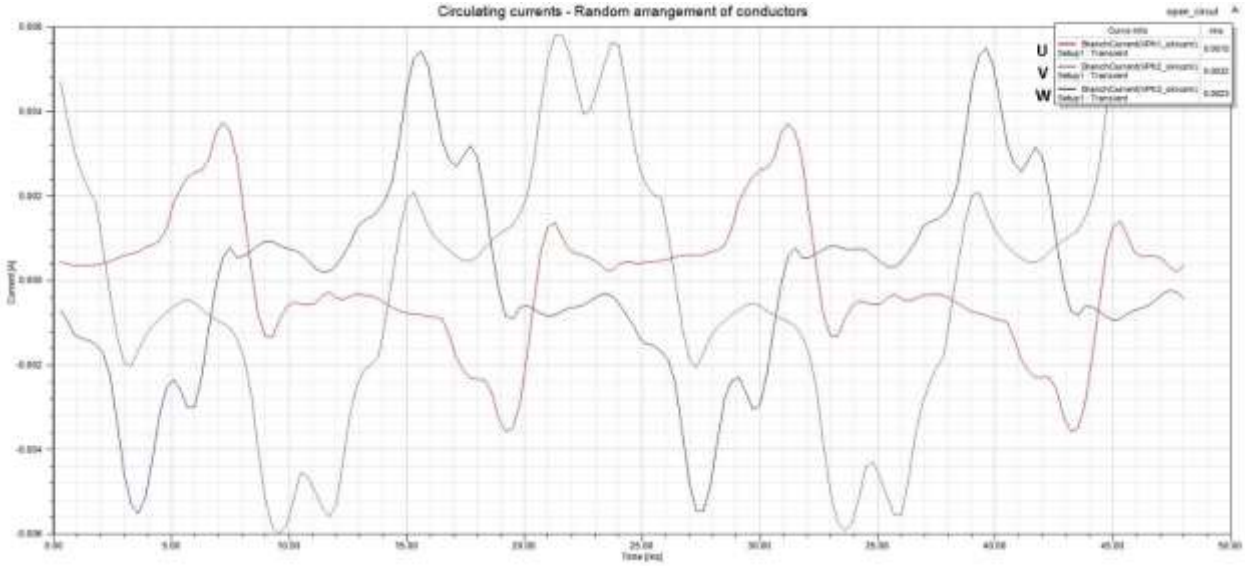

Figure 4. 16 Random arrangement of conductors – Circulating currents OC

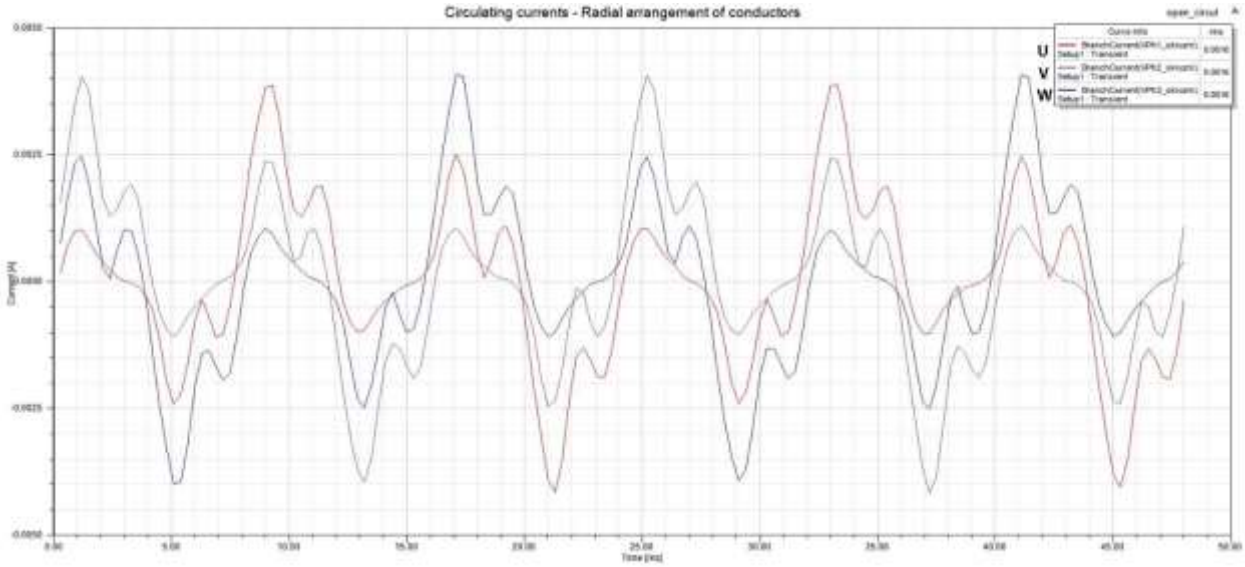

Figure 4. 17 Radial arrangement of conductors – Circulating currents OC

As we can see from Figures 4.16 – 4.18 conductor arrangement poses a big role in waveform shape of circulating currents between strands but RMS of the current is so small, that it makes no effect to Joule's heating in chosen machine. It should be mentioned, that we have only two parallel strands and according to Table 2. With more parallel strand the current could significantly rise. This results support statement in [14], that circulating currents poses small problem according to proximity effect in winding. On the other hand simulation neglected [1] statement, that position of conductors inside slot is insignificant. Their statement will be right only, if we have no parallel strands in winding. Due to symmetry and complexity of model of machine we were able to simulate only strands circulating currents, but no branches circulating currents were simulated.

5.3 FEMM – Current Simulation

In freeware FEMM was also built parametric model of the same machine as in Ansys® Maxwell to compare the results of simulation. Parametric setting was programmed in Lua Script. For LUA commands were used sources [45], [46]. Then the script was lunched in FEMM. We used same parametric model for both machines – parametrization dimensions are in Attachment A.

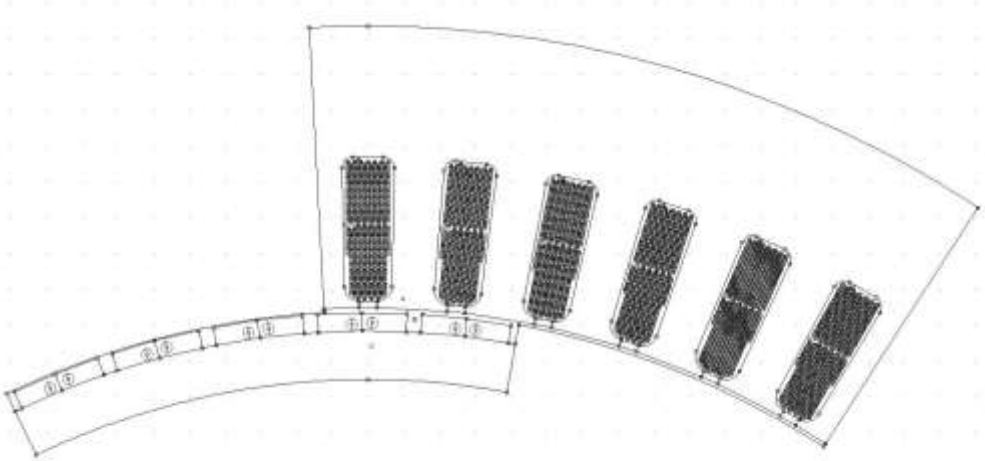

Figure 4. 18 FEMM model of machine

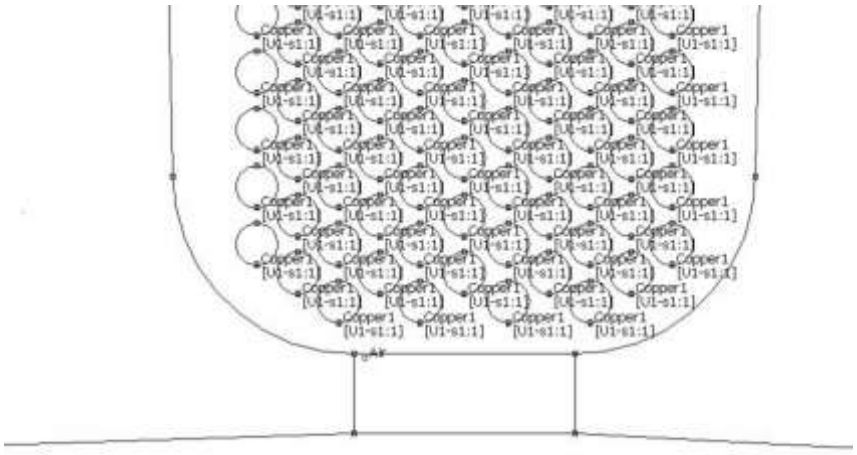

Figure 4. 19 FEMM – detail stator slot

As we can see in Figure 4. 18 and Figure 4. 19 the model is really complex. Every slot was filled with 340 conductors and winding was excited in nominal power operation, where in first phase there is no current and second and third phases are excited by equal current with opposite direction of flow. Precision of mesh was then reduced by settings of model from above 600 000 nodes to 293 000 nodes. This was supposed to reduce solution time. During 5 day of computation on server it was impossible to obtain first approximation of model. Due to this, the model was assumed as unsolvable and for FEMM thermal simulation were used data from Ansys Maxwell, where simulation matches quite properly with catalogue data.

6 THERMAL SIMULATIONS

6.1 Ansys Workbench – Thermal Steady State

From Ansys Maxwell was exported model of machine. After small adjustments in model and setting of material properties from chapter 4.3 we started to simulate thermal model. Due to meshing consumption it was deleted the enamel insulation of copper wire and modified thermal conductivity constant of epoxy resin. In the future, it would be very good to use equivalent insulation system according to [47] to save even more mesh.

The greatest advantage of this software was exporting results of Ohmic losses from Maxwell directly to Ansys 16.0. Due to unexplainable computing problems the software or user error, the calculated temperature drop on ground-wall insulation was only 0.01 °C. Compared with rough analytical calculation (see Attachment B), where temperature drop on ground-wall insulation was 10.8 °C, this simulation was found faulty. During one month process of searching the mistake, it was not found. Due to this problem, it was decided to build only FEMM Thermal simulation.

6.2 FEMM - Thermal simulation – Nominal power

For thermal simulation there were accepted few restrictions and simplifications. **There were neglected rotor core losses and losses of permanent magnets. Also heat dissipation (cooling) through shaft was neglected.** According to thermal simulation [48] in 3D we will assume, that the 2D cut we are watching is exactly in middle of stator packet length, where axial heat dissipation through shaft is smallest.

There were conducted two FEMM simulations. One with analytical input from analytical calculations and the other one with data input from Ansys Maxwell.

6.2.1 Analytical input

For analytical input were used calculations (Attachment B) from nominal current from data sheets of manufacturer. **This simulation calculates only with Joule's losses in winding** caused by nominal current and expects even distribution of current inside each conductor. The heat generation was assigned to the model through losses of material - Watts per cubic meter [W/m^3]. Due to not perfectly working boundary conditions were simulated three slots and the result in middle one is assumed to be relevant.

According to catalogue of manufacturer – water cooling - was used the greatest allowed humidity in environment. For this temperature was found water cooling temperature and was raised by heating of fluid inside machine. Also listed in catalogue. Resulting temperature 55°C was used as boundary in water cooling system. Also boundary in distance of machine in the air was set to 40°C only as a temperature. This boundary setup is not fully proper and it could have been done better.

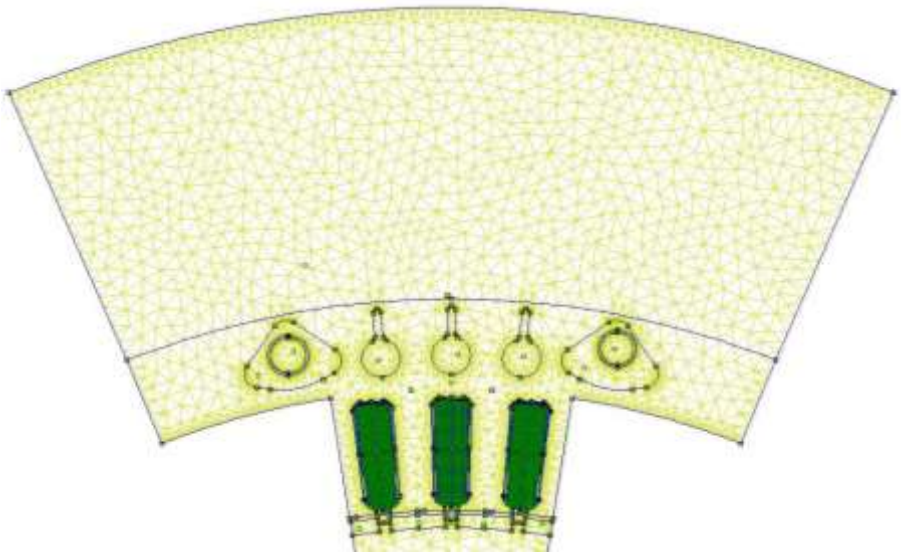

Figure 4. 20 Mesh of thermal model

Figure 4. 20 shows meshing of model. There are three stator slots filled with winding including enamel insulation, epoxy and ground-wall insulation. Two holes on left and right side are used for water cooling. Area above stator sheet is air. All left and right areas (cut outs of the machine) were set with symmetry boundary condition. Problem with missing stator slots on left and right side was solved with heat flux boundary condition equal to heat flux above middle slot.

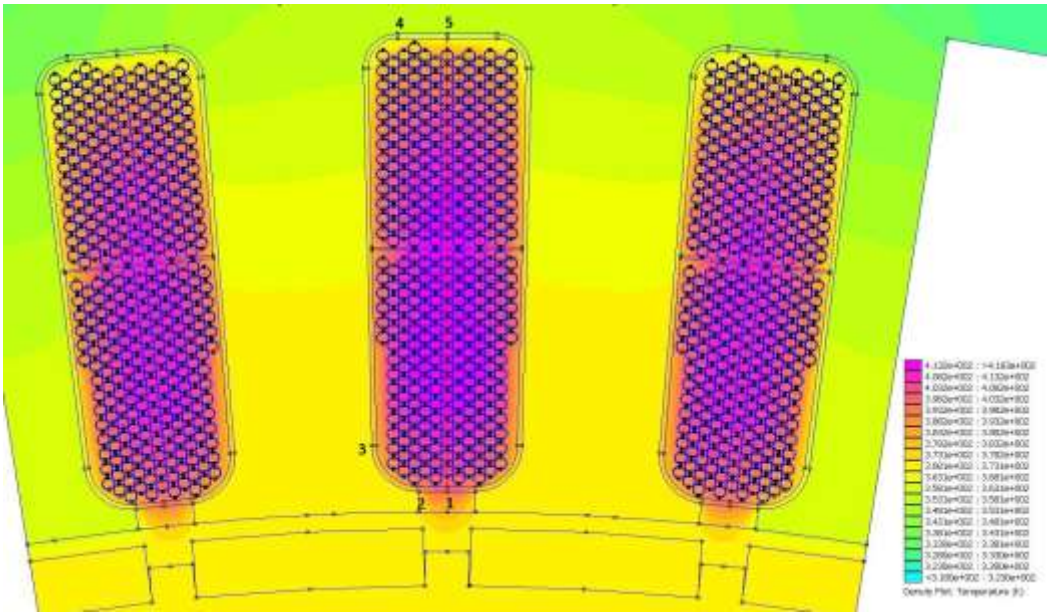

Figure 4. 21 Temperature result of thermal simulation

For verification of results was used very rough analytical calculation of temperature drop on ground - wall insulation presented in (Attachment B). The temperature drop on ground-wall insulation was calculated to 10.8 °C. The calculation assumed unrealistic conditions - homogenous distribution of heat flux along ground-wall insulation and also round shape of stator slot. This calculation was provided only for evaluation of result – if we should expect temperature drop in tenths of a degree or hundreds of degrees.

In Figure 4. 21 are points 1-5 where temperature drop was computed along the perpendicular. The measured temperature drops are shown in following Table 5.

Table 5 Computed and calculated temperature drops across ground-wall insulation

Point	1	2	3	4	5	Analytical calculation
Temperature drop [K]	1.23	15.37	9.06	8.2	10.36	10.8

As we can see in this table and also in Figure 4. 21, the temperature drop in point 1 is really small. This is caused by simulation, where FEMM takes the air as steady matter and not as flowing substance. Normally the temperature drop would be greater in point 1.

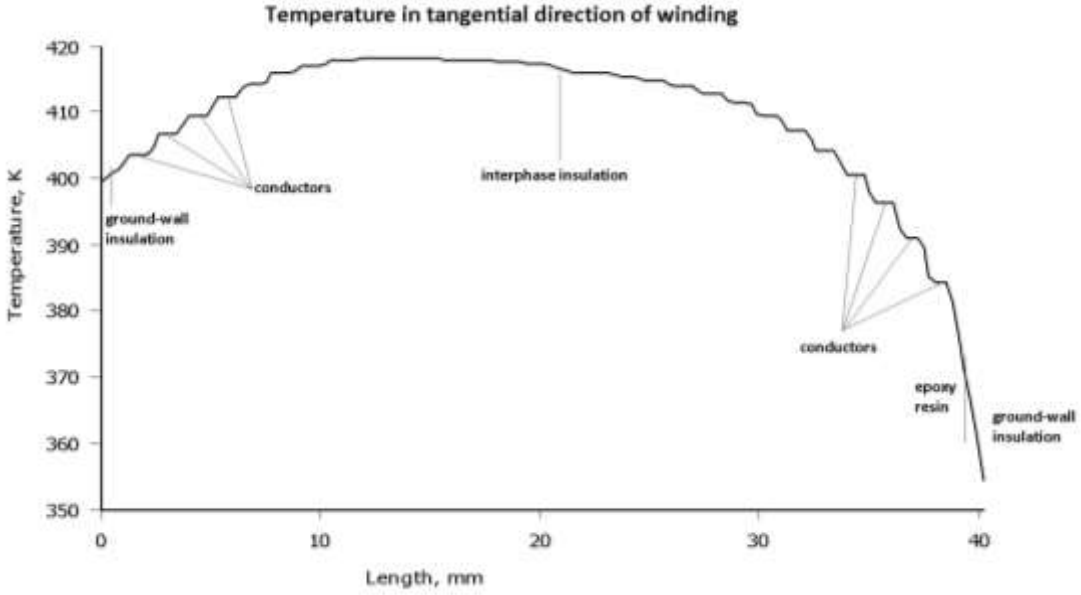

Figure 4. 22 Tangential temperature distribution across line between point 1 and 5 (Figure 4.21)

Figure 4. 22 shows temperature along red line in middle slot in Figure 4. 21. Axis x length begins at the point1 and ends in the point 5. Horizontal temperature flats represents conductors, other temperature drops are on ground-wall insulation, in epoxy-resin, on inter-phase insulation and enamel of wire. The temperature drops are illustrated in the figure above. The enamel temperature drop is not possible to see due to small thickness of enamel. Maximum temperature inside winding according to FEMM is 419 K (145.85 °C).

6.2.2 Maxwell input

Ansys Maxwell was used for results processing and results were manually overwritten to model in FEMM. There were accepted restrictions to make transferring of results time acceptable. Restrictions are explained during the chapter. Model calculates with core losses and Ohmic losses.

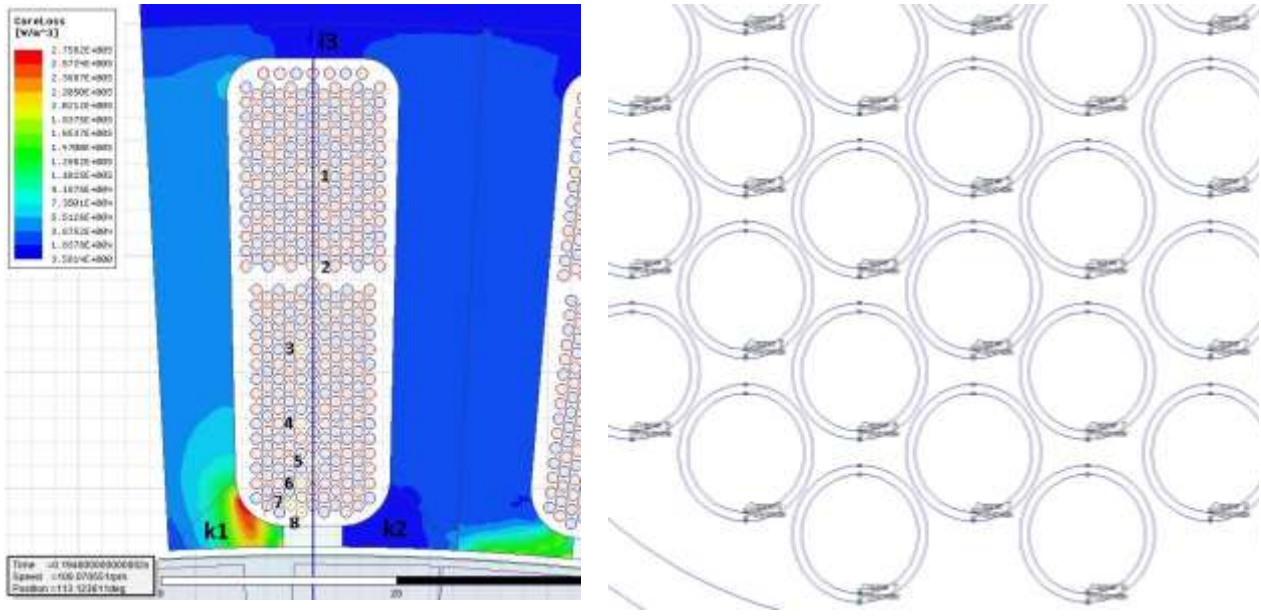

A B

Figure 4. 23 A - Core losses in stator, stator sheet labeling and wire labeling for export, B – FEMM conductors arrangement

Figure 4. 22 A shows prepared model for result processing. The stator sheet was divided to parts k1, k2, i3. There were also selected conductors representing Ohmic losses in whole area above the number or between the numbers. For example all conductors between number 1 and 2 will have assigned Ohmic losses of conductor with number 2. Highest numbers – 8, 7, 6 have pyramid-like shape due to proximity effect in the area of winding. For better understanding just look at the Figure 4. 22 B.

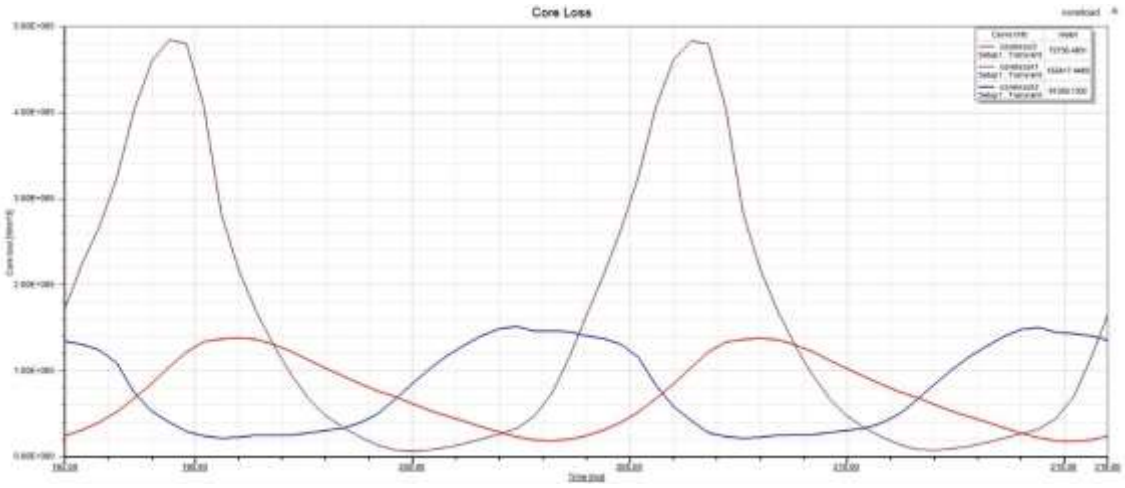

Figure 4. 24 Graph of core losses in Maxwell for transference to FEMM

Core losses in model were integrated through surface and divided by given surface to obtain losses in Watts per cubic meter [$W \cdot m^{-3}$]. Result for each time step of simulation was printed to graph in Figure 4. 24. There is possible to see huge difference between core-losses in leading and trailing edge of stator tooth. In top right corner there is computed mean value of each curve. This mean value of core-losses was used in FEMM simulation for heat generation inside material.

In the same way it was done for conductors with numbers 1-8 marked with yellow color in Figure 4. 22 A, but the difference in Ohmic losses after integration is not so significant. Losses in conductor with number 8 are only 0.6% higher compared with reference conductor number 3. Conductors with numbers 1 and 2 are form different phase of winding with different strand current.

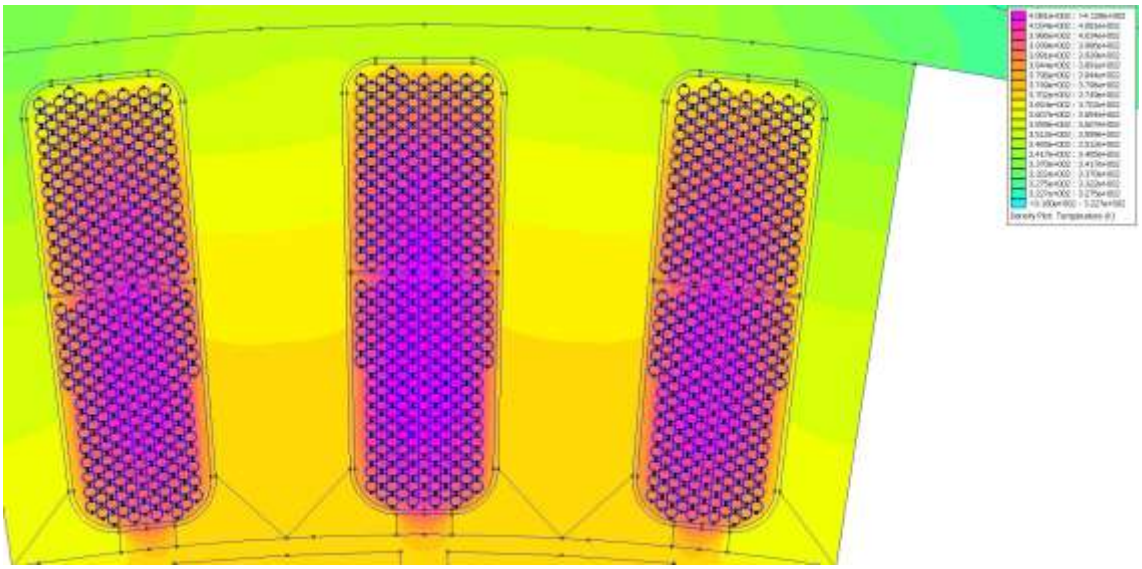

Figure 4. 25 Temperature result of thermal simulation

Figure 4. 25 compared to analytical simulation result in Figure 4. 21 has lower temperatures in winding. This is caused by strand current in Maxwell model, where strand RMS current moves between 5.29 and 5.35 A according to chosen phase and strand of winding. For thermal simulation was chosen the strand with highest current 5.35 A. In analytical calculation in Table 6 was used strand current 5.35 A.

Table 6 Computed and calculated temperature drops across ground-wall insulation

Point	1	2	3	4	5	Analytical calculation
Temperature drop [K]	1.1	13.34	7.86	7.08	8.99	9.7

Including core-losses in thermal model and also lower Ohmic losses reduced temperature drop on ground-wall insulation. Greater deviation from analytical calculation is caused also by core-losses in model. We have to also assume, that temperature drop in point 1 will be greater and in point 2 will be smaller due to air movement in the air gap of machine. So simulation completely does not correspond with real machine.

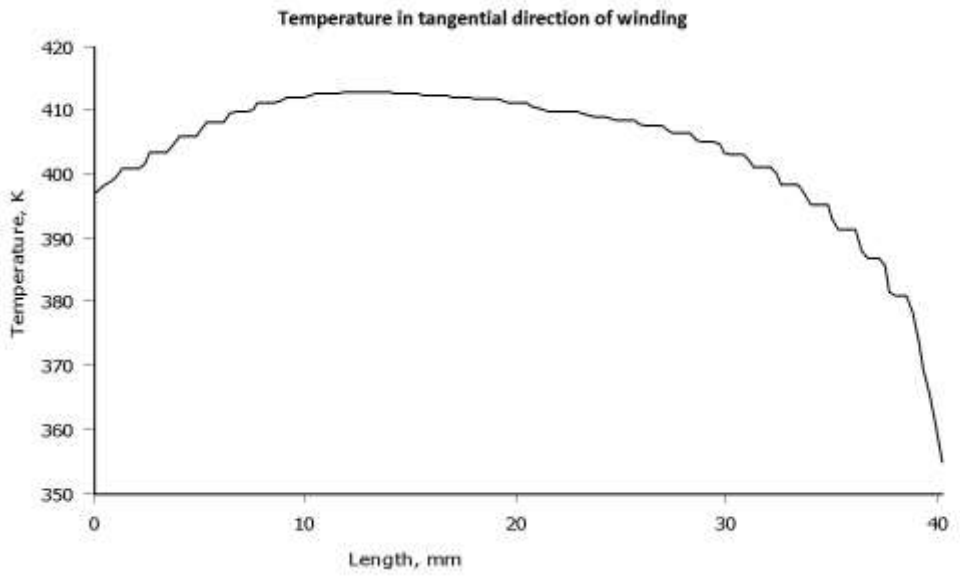

Figure 4. 26 Tangential temperature distribution across line inside winding

Reading of Figure 4. 26 is same as reading of Figure 4. 22. The curves have the same shape, only this figure above has lower temperatures. Maximum temperature inside winding according to FEMM and this graph is 412.8 K (139.65 °C). Temperature difference between hottest points of simulations (analytical vs Maxwell) is 6.2 K.

6.3 FEMM – Selected conductor – Nominal power

Electric time constant and thermal time constant (tau) have a different time range. Due to this we could assume, that temperature inside conductor will not be distributed equally. On the other hand chopper is perfect thermal conductor, so heat conduction in copper itself could spread Ohmic losses equally. This thermal simulation will give us answer.

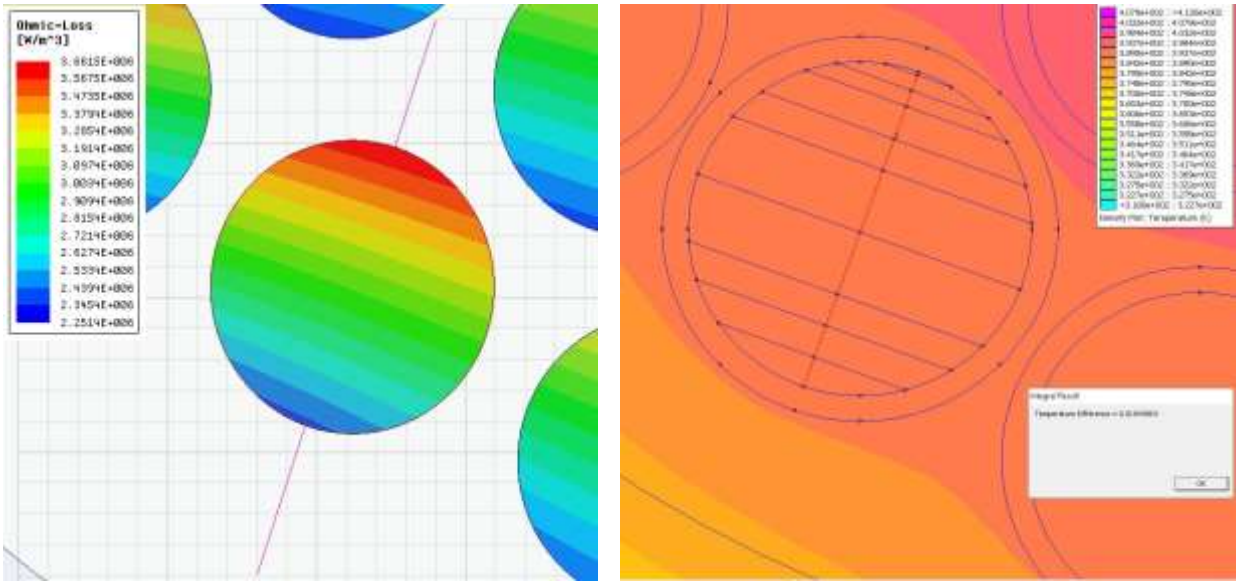

A B

Figure 4. 27 A – Line to display Ohmic-losses in Maxwell, B – complete model in FEMM

It was decided to cut one conductor apart and simulate temperature difference inside one conductor. Integration along surface was impossible due to overlapping of layers in Maxwell and setting of number of turns of coil for the sliced conductor. So we put a straight line crossing through conductor as we can see in Figure 4. 27 A, where mean value was calculated on each curve in different time on restricted length corresponding with length of conductor slice. Mean values for 10 curves in Figure 4. 28 each for different time of period were then manually averaged to resulting Ohmic loss value listed in Figure 4. 29 A on left side.

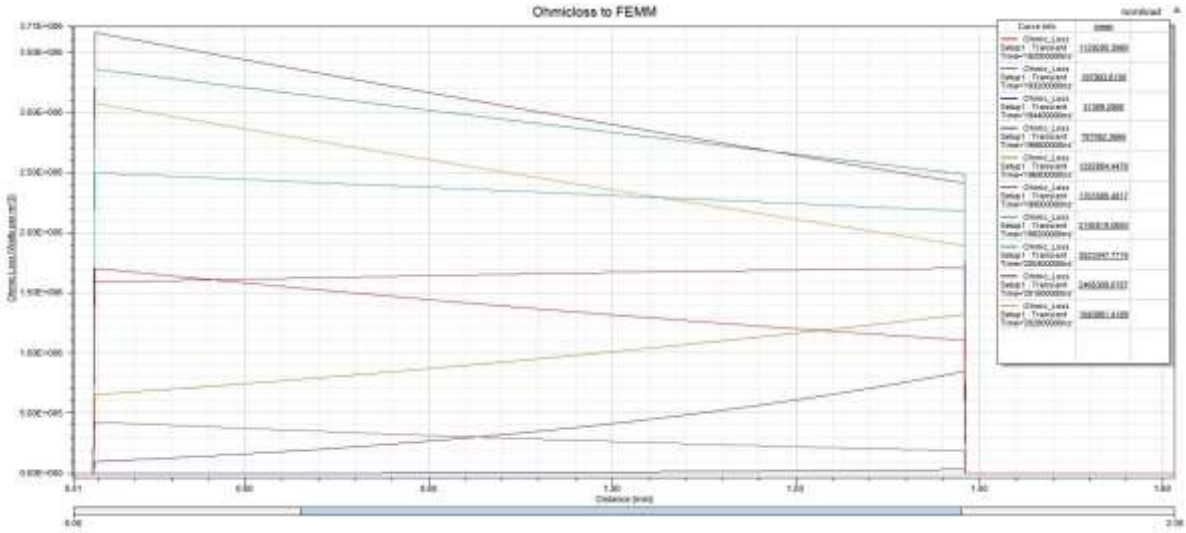

Figure 4. 28 Displayed Ohmic losses along line crossing conductor in Figure 4. 27 - A

Model in FEMM gave us temperature drop 0.01 K as we can see in Figure 4. 27 – B. Temperature drop was computed between beginning of red line and end of red line. Averaged temperature across the conductor is 391.5 K (118.35 °C).

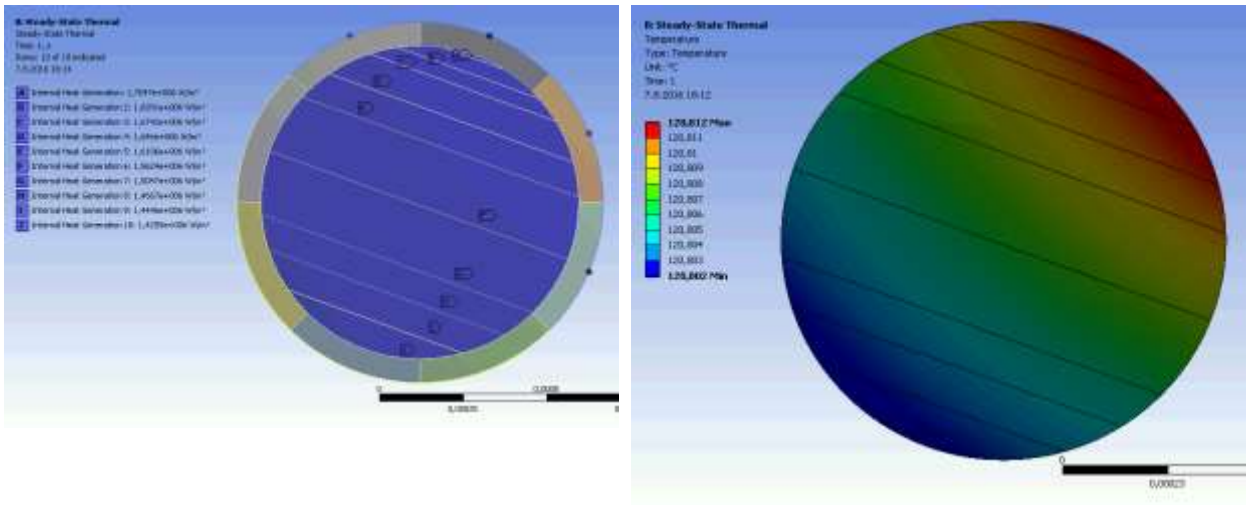

A B

Figure 4. 29 A – Model of single conductor in Ansys 16.0, B – Resulting temperatures

From FEMM model were taken averaged heat flux [$W \cdot m^{-2}$] boundary values to Ansys 16.0 model. The values are averaged along curve of enamel insulation each 45°. Resulting heat flux inflowing to model has blue dots in Figure 4. 29 A, outflowing heat flux has slight yellow line.

Resulting temperatures of model are presented in Figure 4. 29 B. The temperature of conductor in Ansys model is slightly higher 393.95 K (120.8 °C) compared with FEMM model, but temperature difference 0.01 K inside conductor itself matches with FEMM simulation.

As we can see in our case - simulated machine, **the heat flux passing through conductor from the central area of winding is more important on temperature distribution**, than Ohmic losses of proximity effect in conductor itself.

7 FUTURE WORK

In future it would be interesting to investigate influence of 7 parallel strands on circulating currents and proximity effect influence on temperature distribution across conductors in higher frequencies than 43.3 Hz also PWM excitation should be taken into consideration.

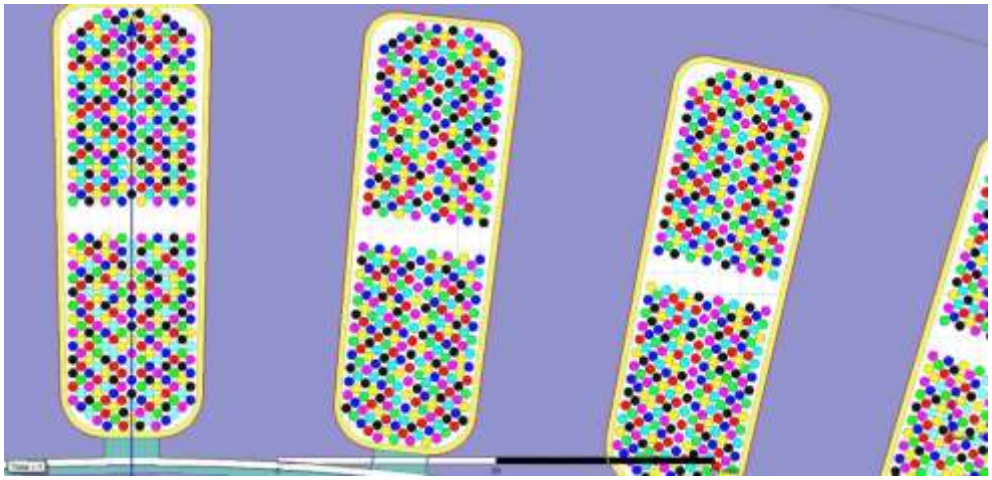

Figure 4. 30 Machine wound with 7 parallel strands

8 CONCLUSION

Thesis tackled with current distribution inside random wound winding of PMSM machine, where conductors are randomly distributed inside stator slot. Simulations were conducted for two operating duty cycles – nominal power and open circuit. The machine type and design sheets was selected by manufacturer. In the end two parallel strands of winding are not enough to cause great current imbalance between parallel strands.

Proximity effect near slot opening was investigated. Influence of permanent magnets from rotor to this effect is significant also coils itself and arrangement of conductors poses a role in this effect as literature search in chapter 3 indicated and results in chapter 4 approved.

The simulations were conducted on the limit level of simulation software environment – FEMM and Maxwell. In Ansys Maxwell many objects (conductors) in modeler caused freezing and jams of screen due to slow search in list of objects. Also software uses only one processor thread for processing of orders in modeler, it was very time-consuming. Due to long solution time of Maxwell models there is noticeable time step of simulation and some inaccuracies occurs. FEMM was not able to solve the electromagnetic model in real time, on the other hand heat flow problem processing was very fast. Ansys 16.0 provides better post-processing tools for thermal simulations than FEMM.

Whole machine and chosen conductor with greatest proximity effect were investigated in chapter 5. Statement of [14], that circulating currents are in comparison with proximity effect almost negligible was approved. Circulating currents between parallel strands were lower than 0.003 A in all models. This “size” of current has minimum influence on Ohmic losses.

On the other hand investigation of proximity effect in conductors was main goal of thesis. The simulations were conducted only with sinusoidal voltage source excitation. According to [18] it is possible to state, that PWM excitation would rise proximity effect in conductors. Following table observes conductor with occurrence of greatest proximity effect. The data were taken from Figure 4. 12, Figure 4. 27 A Figure 4. 29 B.

	Current density [A/mm^2]	Ohmic loss [W/m^3]	Temperature [°C]
Highest value in conductor	8.03	$1.704 \cdot 10^6$	118.38
Lowest value in conductor	7.3	$1.425 \cdot 10^6$	118.37
Difference of values	0.73	$0.279 \cdot 10^6$	0.01
Percentage high/low	110 %	119.6 %	0.008 %

Table 7 Conductor with greatest proximity effect occurrence - summary

Proximity effect in investigated machine was not able to cause temperature imbalance inside observed conductor with proximity effect. Also in Figure 4. 29 B - 3 pages back - we can see, that temperature distribution in winding has different gradient than slices of conductor (current distribution). Through conductor flows heat flux from another conductors in center of stator slot which has greater influence.

Each machine should be evaluated individually due to different excitation frequency and largeness of proximity effect. With higher frequency the phenomena of proximity effect will be more significant.

Thesis brings us insight, that without thermal analysis it is impossible to evaluate possibility of creation of hot-spots in winding, because copper is very good heat conductor. So all articles [2][11][12][14] discussing possibility of creation of hot-spots on conductors of winding due to proximity effect may be or may not be right.

Same as [14] concluded it has to be said, that only conductor level thermal simulations can confirm or disprove creation of hot-spots in winding. In our case (simulated machine) creation of hot-spots was disproved.

BIBLIOGRAPHY

[1] M. S. Islam, S. Mir, and T. Sebastian, "Paralleling the stator coils in permanent magnet machines," *IEEE Int. Conf. Electr. Mach. Drives, 2005.*, pp. 1479–1486, 2005.

[2] M. Popescu and D. G. Dorrell, "Proximity Losses in the Windings of High Speed Brushless Permanent Magnet AC Motors With Single Tooth Windings and Parallel Paths," *Magn. IEEE Trans.*, vol. 49, no. 7, pp. 3913–3916, 2013.

[3] M. Van Der Geest, S. Member, H. Polinder, S. Member, J. a Ferreira, and D. Zeilstra, "Current Sharing Analysis of Parallel Strands in Low-Voltage High-Speed Machines," vol. 61, no. 6, pp. 3064–3070, 2014.

[4] G. Stone, I. Culbert, E. Boulter, and H. Dhirani, *Electrical Insulation for Rotating Machines*, no. 2. 2014.

[5] J. Pyrhonen, T. Jokinen, and V. Hrabovcová, *Design of Rotating Electrical Machines*. 2014.

[6] G. C. Stone, I. M. Culbert, and B. a Lloyd, "Stator Insulation Problems Associated With Low," *Ieee Trans. Ind. Electron.*, pp. 187–192, 2007.

[7] S. U. Haq, "A Study on Insulation Problems in Drive Fed Medium Voltage Induction Motors," 2007.

[8] P. Bernat, "Negativní vlivy měničů frekvence na asynchronní motor," Technická univerzita Ostrava, Fakulta elektrotechniky a informatiky, 2006.

[9] W. Yin, "Failure mechanism of winding insulations in inverter-fed motors," *IEEE Electr. Insul. Mag.*, vol. 13, no. 6, pp. 18–23, 1997.

[10] B. Sonerud, T. Bengtsson, J. Blennow, and S. Gubanski, "Dielectric heating in insulating materials subjected to voltage waveforms with high harmonic content," *IEEE Trans. Dielectr. Electr. Insul.*, vol. 16, no. 4, pp. 926–933, 2009.

[11] H. M. Hämäläinen, J. J. Pyrhönen, and J. Puranen, "Minimizing skineffect in random wound high speed machine stator," no. 2, pp. 752–757, 2009.

[12] S. Iwasaki, R. P. Deodhar, Y. Liu, A. Pride, Z. Q. Zhu, and J. J. Bremner, "Influence of PWM on the proximity loss in permanent-magnet brushless AC machines," *IEEE Trans. Ind. Appl.*, vol. 45, no. 4, pp. 1359–1367, 2009.

[13] A. Młot, M. Korkosz, P. Grodzki, and M. Łukaniszyn, "Analysis of the proximity and skin effects on copper loss in a stator core," *Arch. Electr. Eng.*, vol. 63, no. 2, pp. 211–225, 2014.

[14] M. Popescu and D. G. Dorrell, "Skin effect and proximity losses in high speed brushless permanent magnet motors," *2013 IEEE Energy Convers. Congr. Expo. ECCE 2013*, pp. 3520–3527, 2013.

[15] A. Tessarolo, F. Agnolet, F. Luise, and M. Mezzarobba, "Use of time-harmonic finite-element analysis to compute stator winding eddy-current losses due to rotor motion in surface permanent-magnet machines," *IEEE Trans. Energy Convers.*, vol. 27, no. 3, pp. 670–679, 2012.

[16] M. van der Geest, H. Polinder, J. a. Ferreira, and D. Zeilstra, "Stator winding proximity loss reduction techniques in high speed electrical machines," *2013 Int. Electr. Mach. Drives Conf.*, pp. 340–346, 2013.

[17] P. Zoya and D. Branko, *Introductory electromagnetics*. .

[18] R. Huaytia, "Skin and proximity effect analysis of traction motor," Royal Institute of Technology, School of Electrical Engineering, 2012.

[19] "Skin effect," *Wikipedia: the free encyclopedia*, 2001. [Online]. Available: https://en.wikipedia.org/wiki/Skin_effect. [Accessed: 31-Aug-2015].

[20] E. Jordan and K. Balmain, *Electromagnetic waves and radiating systems*. 1968.

[21] "Elektrisola," 2015. [Online]. Available: http://www.elektrisola.com/hf-litz-wire/terminology-basics/technical-basics-and-calculation.html.

[22] S. Krawczyk, S. Wiak, and X. M. Lopez-Fernandez, "Electromagnetic Fields in Mechatronics, Electrical and Electronic Engineering: Proceedings of ISEF'05," in *Studies in Applied Electromagnetics and Mechanics*, IOS Press, 2006, p. 556.

[23] M. J. Islam, H. V. Khang, a. K. Repo, and a. Arkkio, "Eddy-current loss and temperature rise in the form-wound stator winding of an inverter-fed cage induction motor," *IEEE Trans. Magn.*, vol. 46, no. 8, pp. 3413–3416, 2010.

[24] E. Maruyama, A. Nakahara, A. Takahashi, and K. Miyata, "Circulating current in parallel connected stator windings due to rotor eccentricity in permanent magnet motors," *2013 IEEE Energy Convers. Congr. Expo. ECCE 2013*, pp. 2850–2855, 2013.

[25] a Tenhunen, "Finite-Element Calculation of Unbalanced Magnetic Pull and Circulating Current Between Parallel Windings in Induction Motor With Non-Uniform Eccentric Rotor," no. June, pp. 19–24, 2001.

[26] F. Endert, T. Heidrich, U. Schwalbe, T. Szalai, and S. D. Ivanov, "Effects of current displacement in a PMSM traction drive with single turn coils," 2013.

[27] D. Halliday, R. Resnick, and J. Walker, "Mechanika - Termodynamika," in *Fyzika*, VUTIUM, 2000.

[28] Z. Makki, "OPTIMIZATION OF COOLING SYNCHRONOUS MACHINE," Brno University of Technology, 2016.

[29] M. Janda, "Heat Optimization of Electric Machines," Brno University of Technology, 2008.

[30] T. W. Davies, "Fourier's Law." [Online]. Available: http://www.thermopedia.com/content/781/.

[31] "Temperature Coefficient of Resistance." [Online]. Available: http://www.radio-electronics.com/info/formulae/resistance/resistance-temperature-coefficient.php.

[32] D. Giancoli, "25. Electric Currents and Resistance," in *Physics for Scientists and Engineers with Modern Physics*, New Jersey, 1984.

[33] S. Keppert, *Projektováni elekctrikcých strojů*, 1st ed. Ostrava, 1990.

[34] "Emissivity," *Wikipedia, the free encyclopedia*. [Online]. Available: https://en.wikipedia.org/wiki/Emissivity.

[35] I. P. Kopylov and P. Voženílek, *Stavba elektrických strojů*. Praha: Nakladatelství technické literatury, 1988.

[36] J. P. Karditsas and M. J. Baptiste, "PURE COPPER," *Thermal and Structural Properties of*

Fusion related Materials. [Online]. Available: http://www-ferp.ucsd.edu/LIB/PROPS/PANOS/cu.html.

[37] H. Sa, W. M. Hosny, S. J. Dodds, and D. A. Staton, "Influence of wall insulation material in BPM synchronous servomotor," *Proc. Univ. Power Eng. Conf.*, 2013.

[38] Z. Wang, B. Wu, D. Xu, and N. Zargari, "Dynamic Capacitor Voltage Control of High Power Current Source Converter Fed PMSM Drives for LC Resonance Suppression," pp. 792–797.

[39] "DuPont ™ Kapton ® MT," 2014.

[40] "DuPont ™ Nomex ® Paper Type 410," 2013.

[41] S. Diaham, D. Mary, and D. Malec, "Thermal Breakdown Modeling in Polyimide Films by Solving the Heat Balance Equation," pp. 975–978, 2013.

[42] "Specific Heat Capacity Measurements Using DSC I -," 1981.

[43] W. Tong, *Mechanical Design of Electric Motors*. 2014.

[44] F. Lin, G. S. Bhatia, and J. D. Ford, "Thermal conductivities of powder-filled epoxy resins," *J. Appl. Polym. Sci.*, vol. 49, no. 11, pp. 1901–1908, 1993.

[45] D. Meeker, "Finite element method magnetics," 2015.

[46] I. Hahn, "Einführung in FEMM," Erlangen, 2016.

[47] A. Boglietti, E. C. Member, M. Cossale, S. Member, M. Popescu, D. Staton, S. Vaschetto, and I. I. I. Ntroduction, "Equivalent Thermal Conductivity Determination of Winding Insulation System by Fast Experimental Approach," pp. 1215–1220, 2015.

[48] D. G. Nair, "Coupled Analytical and 3D Numerical Thermal Analysis of a TEFC Induction Motor," pp. 3–8, 2015.

ATTACHMENTS

ATTACHMENT A – Chosen Parametric Dimensions of Machine

List of parametric dimensions:

d_sb – slot bottom diameter [mm]
di_s – stator inner diameter [mm]
di_sh – shaft inner diameter [mm]
dm_rs1 – stator slot circle center pitch 1 [mm]
dm_rs2 – stator slot circle center pitch 2 [mm]
do_r – rotor outer diameter (do_r = do_rm + 2 · h_mg) [mm]
do_rs – rotor outer diameter of sheet [mm]
do_rm – rotor outer diameter under magnet [mm]
do_s – stator outer diameter [mm]
fi – angle of stator slot tooth slope (in view of [0,0]) [deg]
h_mg – magnet height [mm]
h_sbot- slot bottom height [mm]
h_shead – slot head height [mm]
h_so – slot opening height [mm]
i_th – thickness of ground-wall insulation [mm]
r_s1 – slot corner radius 1 [mm]
r_s2 – slot corner radius 2 [mm]
rfi – angle of one polygon part [deg]
w_mg – permanen magnet width [mm]
w_so - slot opening width [mm]

Stator slot

S0! - [0; di_s·0,996/2]
S1! - [-w_so/2; di_s·0,996/2]
S2 - [-w_so/2; di_s/2+h_so]
S3 - [-dm_rs1/2-(rs_1·cos(pi/4)); di_s/2+h_shead-(r_s1·sin(pi/4))]
S4 - [-dm_rs1/2-(r_s1·cos(fi)); di_s/2+h_shead-(r_s1·sin(fi))]
S5 - [-dm_rs2/2-(r_s2·cos(fi)); di_s/2+h_sbot-(r_s2·sin(fi))]
S6 - [-dm_rs2/2-(rs_2·cos(pi/4)); di_s/2+h_sbot+(r_s2·sin(pi/4))]
S7 - [-dm_rs2/2; d_sb/2]
S8 - [0; d_sb/2]
S9 - [-dm_rs1/2; di_s/2+h_shead]
S10 - [-dm_rs1/2; di_s/2+h_shead]
! = dimension is gained by coefficient due to proper function of cutting tool of object in Ansys Maxwell.

Stator insulation

Si1 - [-w_so/2; di_s/2+h_so+i_th]
Si2 - [-dm_rs1/2-(rs_1·cos(pi/4))+i_th·sin(pi/4); di_s/2+h_shead-(r_s1·sin(pi/4))+i_th·sin(pi/4)]
Si3 - [-dm_rs1/2-(r_s1·cos(fi))+i_th; di_s/2+h_shead-(r_s1·sin(fi))]
Si4 - [-dm_rs2/2-(r_s2·cos(fi))+i_th; di_s/2+h_sbot-(r_s2·sin(fi))]
Si5 - [-dm_rs2/2-(rs_2·cos(pi/4))+i_th; di_s/2+h_sbot+(r_s2·sin(pi/4))]
Si6 - [-dm_rs2/2; d_sb/2-i_th]
Si7 - [0; d_sb/2-i_th]

Rotor

R1 - [0; do_rs/2]
R2 - [r_tw/2; do_rs/2]
R3 - [r_tw/2; (cos(rfi)-1)/sin(rfi)·r_tw/2+do_rm/2]
R4 - [do_rm/2·sin(rfi); do_rm/2·cos(rfi)]
R5 - [do_rm/2·sin(2·rfi); do_rm/2·cos(2·rfi)]

Magnets

M1 - [do_rm/2·sin(rfi)-w_mg·cos(rfi/2); do_rm/2·cos(rfi)+w_mg·sin(rfi/2)]
M2·
M3 - [do_rm/2·sin(rfi)+h_mg·sin(rfi/2); do_rm/2·cos(rfi)+h_mg·cos(rfi/2)]
M4 - [do_rm/2·sin(rfi); do_rm/2·cos(rfi)]
M21 - [do_rm/2·sin(rfi); do_rm/2·cos(rfi)]
M22 - [do_rm/2·sin(rfi)+h_mg·sin(rfi+rfi/2); do_rm/2·cos(rfi)+h_mg·cos(rfi+rfi/2)]
M23·
M24 - [do_rm/2·sin(rfi)+w_mg·cos(rfi+rfi/2); do_rm/2·cos(rfi)-w_mg·sin(rfi+rfi/2)]
· = Points were not necessary during creation of parametric model.

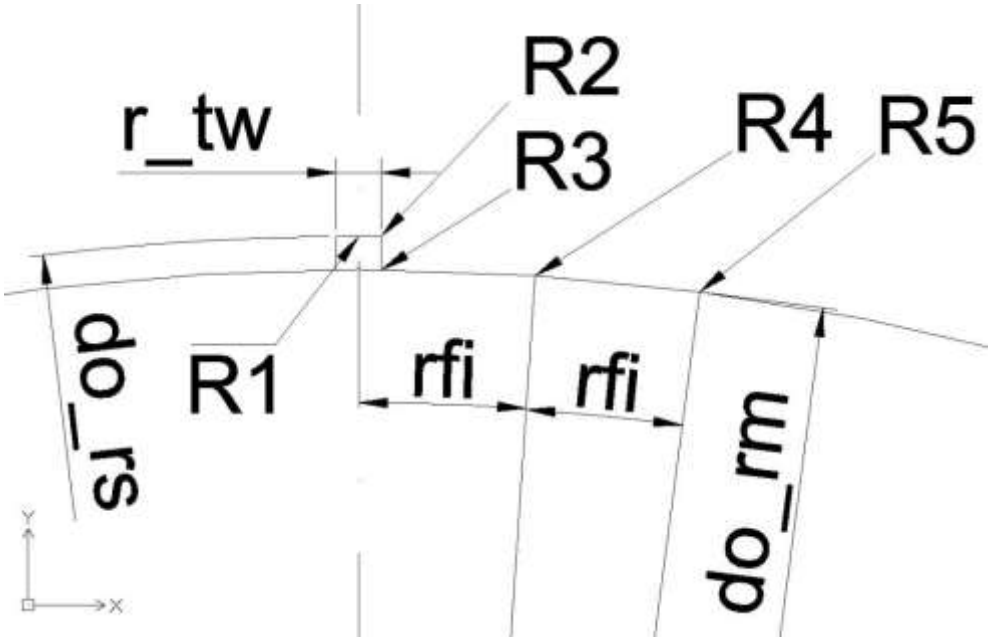

Parametric dimensions of rotor and chosen points

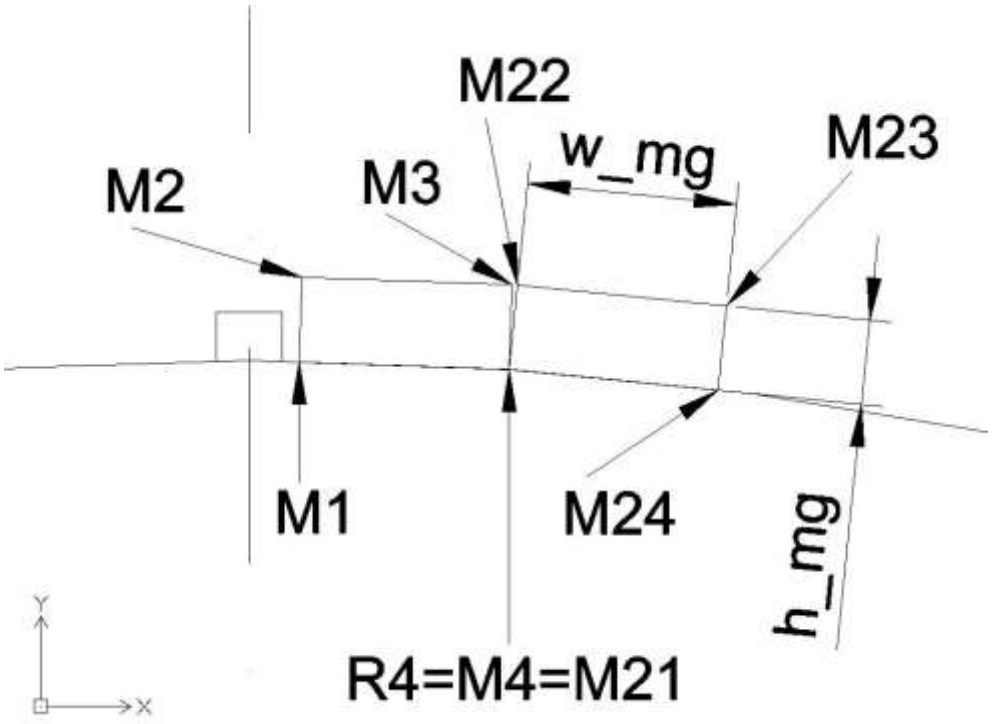

Parametric dimensions of magnets and chosen points

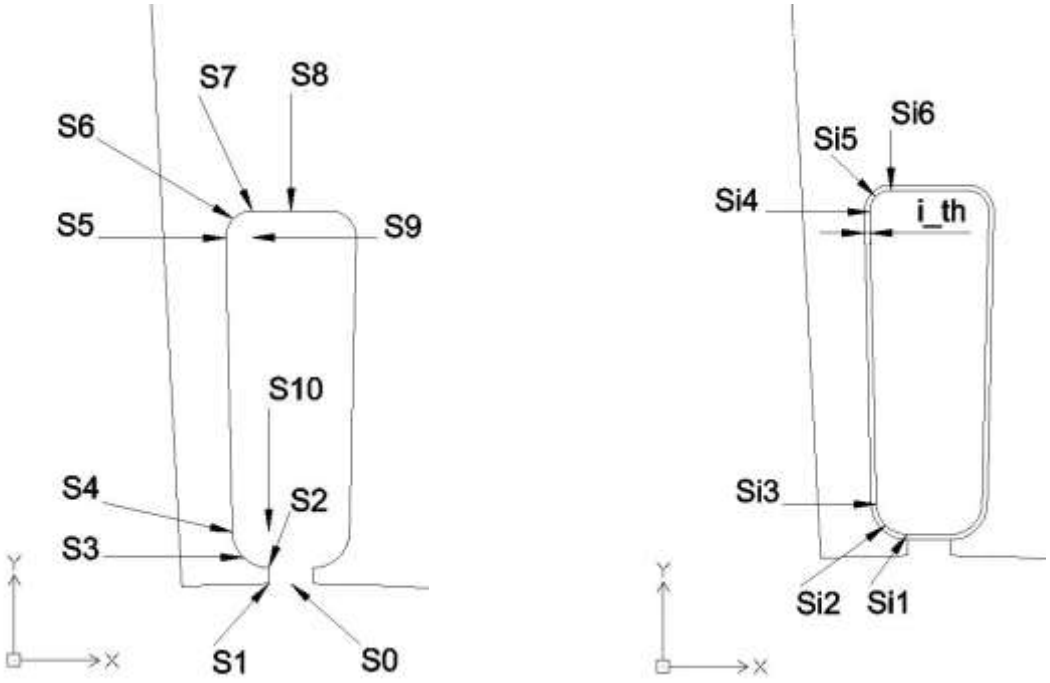

Parametric points of stator slot and ground-wall insulation

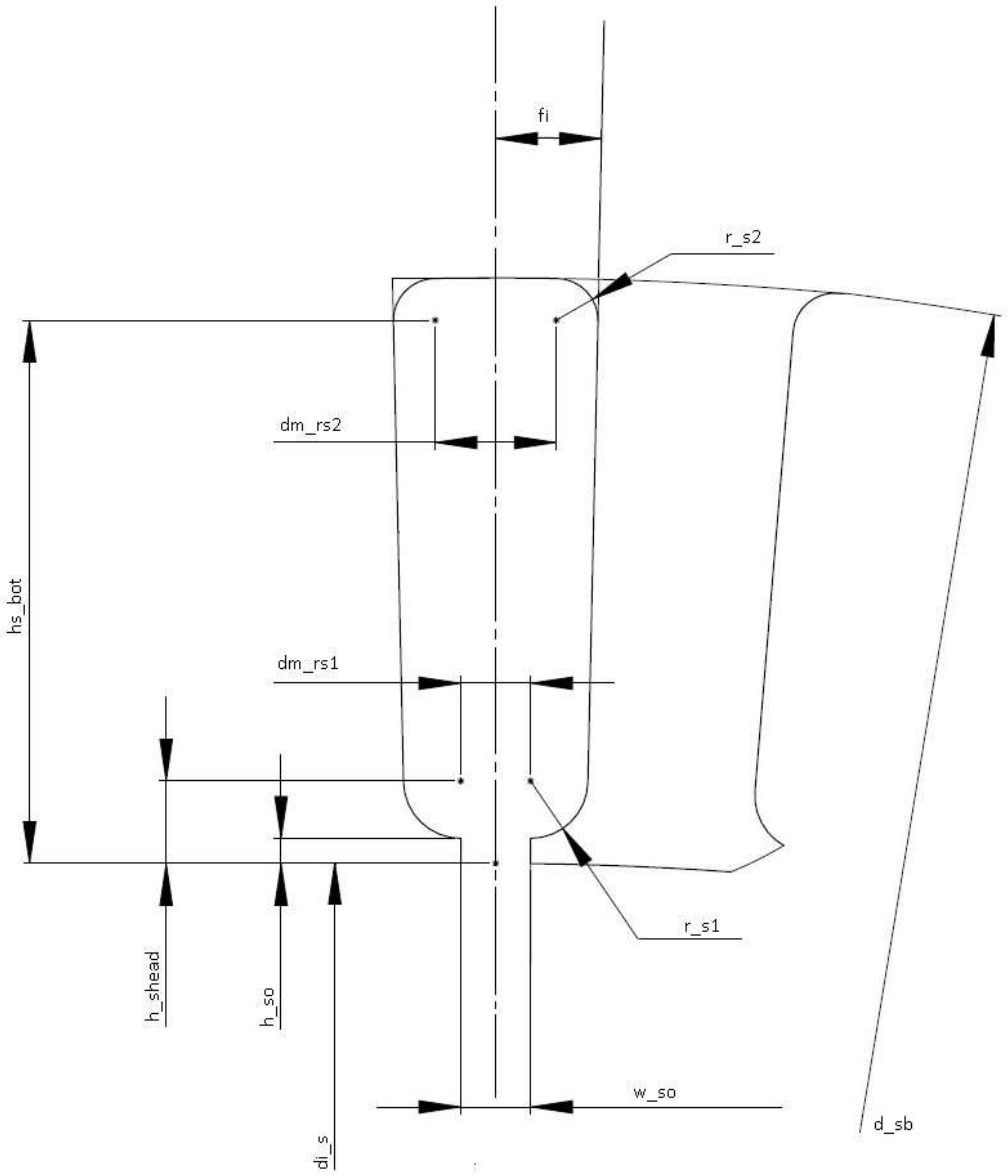

Parametric dimensions of stator

ATTACHMENT B – Analytical Calculations

Analytical Calculation of Conductor DC losses

I_n = 111 A nominal load current, Y winding, 10 parallel coils, each coil wound from 2 parallel strands, thermal class insulation H = °180 °C (Permited average winding temperature = 165 °C, see *Table 1* in thesis)

x = 0.306 m – length of stator slot, d = 0.95 mm diameter of Cu wire (S_{Cu} = 0.70882 mm^2)

$\rho_{20°C}$ = 1.72·10^{-8} Ω·m, α_{Cu} = 0.003862 K^{-1}

Current in one parallel strand (one conductor)

$$I_{1c} = \frac{I_n}{par.\ coils \cdot strands} = \frac{111}{10 \cdot 2} = 5.55\ A$$

Electrical resistivity of copper for 165°C

$$\rho_{165\,°C} = \rho_{20°C} \cdot (1 + \alpha \cdot {}_{\Delta}T) = 1.72 \cdot 10^{-8} \cdot \left(1 + 0.003862 \cdot (165 - 20)\right) = 2.6832 \cdot 10^{-8}\ \Omega \cdot m$$

Electric resistence

$$R_{DC} = \frac{\rho_{180\,°C} \cdot x}{S_{cu}[m^2]} = \frac{2.6832 \cdot 10^{-8} \cdot 0.306}{0.70882 \cdot 10^{-6}} = 11.583\ m\Omega$$

Joule heating in one conductor

$${}_{\Delta}P_{cu\,DC} = R_{DC} \cdot {I_{1c}}^2 = 0.011583 \cdot 5.55^2 = 0.3568\ W$$

Heating per cubic metre for FEMM model

$$Q = \frac{{}_{\Delta}P_{cu\,DC}}{x \cdot S_{cu}[m^2]} = \frac{0.3568}{0.306 \cdot 070882 \cdot 10^{-6}} = 1.645 \cdot 10^6\ W/m^3$$

Analytical Calculation of temperature drop on groundwall insulation

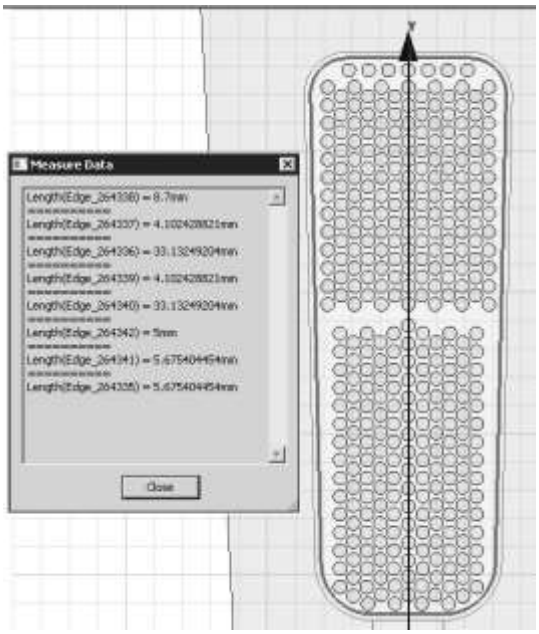

th = 0.00043 m - groundwall insulation thickness

λ = 0.164 $Wm^{-1}K^{-1}$ - thermal conductivity of groundwall insulation

y = 99,51 mm - length of perimeter of insulation

τ = 1 s – time

n_c = 340 – number of conductors in slot

Heat generated in conductors in single stator slot

$$Q = {}_{\Delta}P_{cu\,DC} \cdot n_c \cdot \tau = 0.37005 \cdot 340 \cdot 1 = 125.817\ J$$

Area of groundwall insulation

$$A = y \cdot x = 99.51 \cdot 306 = 0.03045\ m^2$$

Heat flux through groundwall insulation

$$q = \frac{Q}{\tau \cdot \mathrm{A}} = \frac{125{,}817}{1 \cdot 0.03045} = 4131.92\ Wm^{-2}$$

Temperature drop on groundwall insulation

$${}_{\Delta}T = \frac{q \cdot th}{\lambda} = \frac{4131.92 \cdot 0{,}00043}{0.164} = 10{,}8\ K$$